PASJ: Publ. Astron. Soc. Japan , 1–??,
© 2016. Astronomical Society of Japan.

arXiv:1610.05439v2 [astro-ph.SR] 19 Oct 2016

Photospheric carbon and oxygen abundances of F–G type stars in the Pleiades cluster *

Yoichi Takeda[1,2], Osamu Hashimoto[3], and Satoshi Honda[4]
[1]*National Astronomical Observatory, 2-21-1 Osawa, Mitaka, Tokyo 181-8588*
takeda.yoichi@nao.ac.jp
[2]*SOKENDAI, The Graduate University for Advanced Studies, 2-21-1 Osawa, Mitaka, Tokyo 181-8588*
[3]*Gunma Astronomical Observatory, 6860-86 Nakayama, Takayama, Agatsuma, Gunma 377-0702*
[4]*Nishi-Harima Astronomical Observatory, Center for Astronomy, University of Hyogo, 407-2 Nishigaichi, Sayo-cho, Sayo, Hyogo 679-5313*

(Received 2016 September 6; accepted 2016 October 13)

Abstract

In order to investigate the carbon-to-oxygen ratio of the young open cluster M 45 (Pleiades), the C and O abundances of selected 32 F–G type dwarfs (in the effective temperature range of $T_{\rm eff} \sim 5800$–7600 K and projected rotational velocity range of $v_{\rm e}\sin i \sim 10$–110 km s^{-1}) belonging to this cluster were determined by applying the synthetic spectrum-fitting technique to C I 5380 and O I 6156–8 lines. The non-LTE corrections for these C I and O I lines were found to be practically negligible (less than a few hundredths dex). The resulting C and O abundances (along with the Fe abundance) turned out nearly uniform without any systematic dependence upon $T_{\rm eff}$ or $v_{\rm e}\sin i$. We found, however, in spite of almost solar Fe abundance ([Fe/H] ~ 0), carbon turned out to be slightly subsolar ([C/H] ~ -0.1) while oxygen slightly supersolar ([O/H] $\sim +0.1$). This lead to a conclusion that [C/O] ratio was moderately subsolar (~ -0.2) in the primordial gas from which these Pleiades stars were formed ~ 120–130 Myr ago. Interestingly, similarly young B-type stars are reported to show just the same result ([C/O] ~ -0.2), while rather aged ($\sim$ 1–10 Gyr) field F–G stars of near-solar metallicity yield almost the solar value ([C/O] ~ 0) on the average. Such a difference in the C/O ratio between two star groups of distinctly different ages may be explained as a consequence of orbit migration mechanism which Galactic stars may undergo over a long time.

Key words: open clusters and associations: individual (M 45) — stars: abundances — stars: atmospheres — stars: solar-type

1. Introduction

The abundances of carbon and oxygen in the Galaxy are currently attracting hot interest of astrophysicists, because they play significant roles in the chemical characteristics of celestial objects such as stars and planets. For example, carbon-dominated rocky planets (rather than oxygen-dominated ones such as those existing in the solar system) are expected to form if C/O ratio of the circumstellar gas is sufficiently high to satisfy $N({\rm C})/N({\rm O}) > 0.8$ (e.g., Bond et al. 2010), which corresponds to [C/O] $> +0.16$ if Asplund et al.'s (2009) solar abundances of $A_\odot({\rm C}) = 8.43$ and $A_\odot({\rm O}) = 8.69$ are adopted.[1] Accordingly, the primary issue is whether such stars with appreciably supersolar [C/O] ratio ([C/O] $\gtrsim 0.2$) exist or not, which can be checked by examining spectroscopically determined C and O abundances of solar-type stars. Generally speaking, rather metal-rich stars would be promising for such candidates, because [C/O] values observed in F–G stars in the Galactic disk tend to rise over zero at [Fe/H] $\gtrsim 0$ as a result of slower decreasing rate of [C/Fe] than [O/Fe] with an increase of [Fe/H] (see, e.g., Fig. 7 of Gustafsson et al. 1999, or Fig. 6d in Takeda & Honda 2005).

However, despite that several groups challenged this problem recently, considerably discordant results have been reported: Delgado Mena et al. (2010) as well as Petigura and Marcy (2011) argued that a significant fraction ($\sim$ 20–30%) of nearby FGK stars have $N({\rm C})/N({\rm O}) > 0.8$ (even $N({\rm C})/N({\rm O}) > 1$ is found for $\gtrsim 5$% of the sample). On the other hand, Nissen et al. (2014) criticized the consequences of these two studies as being questionable (presumably due to the difficult nature of adopted forbidden [O I] 6300 line which suffers a blending with Ni I line and has a different parameter-sensitivity in comparison to the high-excitation C I lines also used by them), and concluded based on high-excitation C I 5052/5380 and O I 7771–5 lines that very few F–G stars in the solar neighborhood exceed the critical $N({\rm C})/N({\rm O})$ limit of 0.8 even

* Based on data collected by using the 1.5-m Telescope of Gunma Astronomical Observatory, and those with the 1.88-m Telescope of Okayama Astrophysical Observatory (obtained from SMOKA, operated by the Astronomy Data Center, National Astronomical Observatory of Japan).

[1] In this paper, we define the logarithmic number abundance for element X as $A({\rm X}) \equiv \log[N({\rm X})/N({\rm H})] + 12$, where $N({\rm X})$ and $N({\rm H})$ is the number density of element X and H (hydrogen), respectively. Similarly, we use the usual notation for the differential logarithmic abundance ratio relative to the Sun: $[{\rm X/Y}]_* \equiv [{\rm X/H}] - [{\rm Y/H}] \equiv [A_*({\rm X}) - A_\odot({\rm X})] - [A_*({\rm Y}) - A_\odot({\rm Y})]$, where the subscripts "*" and "$\odot$" mean "object" and "Sun", respectively.

at the highest metallicity of [Fe/H] = +0.4. Furthermore, Nakajima and Sorahana (2016) very recently examined the distribution of C-to-O abundance ratio of M dwarfs, and lent support rather to the latter conclusion of Nissen et al. (2014). In any event, more observational studies would be needed to settle this controversy.

In this connection, investigating the C and O abundances of stars belonging to an open cluster is of significance, since (1) they represent the original composition of the gas at a well-established time point in the Galactic history and (2) fairly accurate abundances are determinable by comparing/averaging the results of many members by making use of the chemical homogeneity. Takeda et al. (2013; hereinafter referred to as Paper I) once studied the C and O abundances of F–G stars in the Hyades cluster (age of $\sim$ 625 Myr; cf. Perryman et al. 1998). Interestingly, as remarked in Sect. 6.2 therein, a slightly subsolar [C/O] (~ -0.1) was obtained, despite that this cluster is somewhat metal-rich ([Fe/H] $\sim$0.1–0.2) and expected to have a trend of [C/O] $\gtrsim 0$ according to the [C/O]–[Fe/H] relation mentioned above (derived from field FGK stars with ages of $\sim$1–10 Gyr). Does any different tendency holds for the [C/O] ratios of rather young cluster stars?

In view of this consideration, it is meaningful to check the C and O abundances of another well-known open cluster M 45 (Pleiades), which has an age of $\sim$ 120–130 Myr (cf., Basri, Marcy, & Graham 1996; Bonatto, Bica, & Girardi 2004) and thus further younger than Hyades. Unfortunately, available previous investigations of C and O abundances in the Pleiades stars are not so many, despite that various spectroscopic studies of other elements have been published (see, e.g., Table I of Gebran & Monier 2008 or Sect. 1 of Funayama et al. 2009) where the metallicity ([Fe/H]) was reported to be nearly solar.

— Friel and Boesgaard (1990) determined the C abundances for 12 Pleiades dwarfs ($T_{\rm eff} \sim$ 5900–6900 K) by using C I 7771–9 and C I 6587 lines and derived an almost near-solar (or very slightly subsolar) tendency for [C/H] (-0.06).

— Boesgaard (2005) reported that the C and O abundances of 20 late-F and early-G stars ($T_{\rm eff} \sim$ 5600–6200 K) determined from C I 7111–9 and O I 7771–5 lines were almost solar (the mean abundances were $\langle$[C/H]$\rangle = -0.02$ and $\langle$[O/H]$\rangle = +0.01$).

— Gebran and Monier (2008) carried out abundance studies for 21 stars (16 A-type and 5 F-type) of the Pleiades cluster for 18 elements including C and O. By using a spectrum-fitting technique applied to a number of C I and O I lines, they found that C and O tend to be underabundant relative to the Sun, where the extent of deficiency is larger for A stars ($-0.5 \lesssim$ [C/H] $\lesssim +0.2$ and $-0.4 \lesssim$ [O/H] $\lesssim +0.2$) than F stars ($-0.1 \lesssim$ [C/H] $\lesssim 0.0$ and $-0.3 \lesssim$ [O/H] $\lesssim 0.0$). We should bear in mind, however, that light-element abundances of A-type stars may suffer chemical anomalies due to the diffusion process in the outer layer.

These previous studies suggest that C and O abundances of Pleiades are not so much different from the solar composition and thus precise determination of the C/O ratio in this young cluster needs a careful analysis. Motivated by this situation, we decided to contend with this problem by conducting new determinations of C and O abundances for selected 32 Pleiades F–G type stars, with an aim of clarifying the characteristics regarding [C/H], [O/H], and [C/O] of this young cluster. This is the purpose of this investigation.

The remainder of this article is organized as follows. After describing our observational data in section 2, we explain the assignments of atmospheric parameters in section 3. The procedure of our abundance determination based on the spectrum-fitting method is illustrated in section 4. Section 5 discusses the consequence of our analysis, where the resulting abundances of C and O along with the C/O ratios of the Pleiades stars are examined in various respects. In addition, two supplementary sections are prepared to justify the adopted reference solar oxygen abundance derived from the O I 6156–8 lines (appendix 1) and to briefly report the Li abundances of 7 Pleiades stars among our sample (appendix 2).

2. Observational data

A total of 32 F–G dwarfs of the Pleiades cluster were selected as the sample stars of this study. Regarding 25 stars among them, we made use of the high-dispersion spectral data (with a spectral resolving power of $R \sim 40000$) in the green–red region originally obtained in 2006–2007 by Funayama et al. (2009) and employed for their metallicity study of Pleiades stars, which are archived as raw (unprocessed) data at Gunma Astronomical Observatory (GAO) and Okayama Astrophysical Observatory (OAO). See Sect. 2 in Funayama et al. (2009) regarding the observational details of these data.

In addition, we newly carried out spectroscopic observations of 7 stars in the 2015–2016 season by using GAOES (Gunma Astronomical Observatory Echelle Spectrograph) installed at the Nasmyth Focus of the 1.5 m reflector of GAO, by which $R \sim 40000$ spectra (corresponding to the slit width of 2″) covering the wavelength range of 5340–6580 Å were obtained.

The data reduction for all these 32 stars (bias subtraction, flat-fielding, aperture-determination, scattered-light subtraction, spectrum extraction, wavelength calibration, and continuum-normalization) was performed using the "echelle" package of IRAF.[2] Generally, a number of spectral frames (sometimes those obtained over several different nights)[3] for each star were co-added in order to improve the data quality. The typical S/N ratio of the

[2] IRAF is distributed by the National Optical Astronomy Observatories, which is operated by the Association of Universities for Research in Astronomy, Inc., under cooperative agreement with the National Science Foundation.

[3] Regarding MSK 65 (= HII 761), since the radial velocity of this star was found to be considerably variable with a short time scale, we had to correct the wavelength scale of each spectrum to the laboratory frame before co-addition.

resulting spectra is around ~ 100 (i.e., $\sim$ 40–50 for the worst cases while ~ 150 for the best cases) . The basic information of the finally adopted observational data for our 32 sample stars (along with their photometric data taken from the SIMBAD database) is summarized in table 1.

Besides, since we selected Procyon (F5 III–IV) and Sun (Moon) as the reference stars, their spectra were taken from Takeda et al.'s (2005a) spectrum database of 160 FGK stars which were obtained at OAO.[4]

3. Atmospheric parameters

The fundamental atmospheric parameters [the effective temperature ($T_{\rm eff}$), logarithmic surface gravity ($\log g$), microturbulence (ξ)] of each 32 Pleiades star were determined by making use the fact that all the objects (member stars of the Pleiades cluster) are known to have almost the same age ($\sim$ 120–130 Myr) and the solar abundance (cf. section 1). We adopted the solar-metallicity isochrones[5] computed by Bressan et al.'s (2012, 2013) PARSEC code (version 1.2S) corresponding to the age of 125 Myr,[6] in which the values of M_{V0} (absolute visual magnitude), $(B-V)_0$ (unreddened color), $T_{\rm eff}$, and g are tabulated in terms of the stellar mass. These data suffice us to express M_{V0}, $T_{\rm eff}$, and $\log g$ in terms of $(B-V)_0$, which was derived from the observed $B-V$ color (taken from the SIMBAD database) along with the typical color excess of $E_{B-V}=0.03$ mag (or the extinction is $A_V=3.1E_{B-V}=0.093$ mag) for the Pleiades cluster (see Table 3 of Breger 1986). The $V_0(\equiv V-A_V)$ vs. $(B-V)_0$ plots for the program stars are compared with the isochrones (where M_{V0} was reduced to V_0 by using the distance of 136.2 pc; cf. Melis et al. 2014) in figure 1a. The final $T_{\rm eff}$–$(B-V)_0$ and $\log g$–$(B-V)_0$ relations we adopted for our Pleiades stars are shown (by solid lines) in figures 1b and 1c, respectively, where other empirical formula occasionally used for FGK dwarfs are also shown (by dashed lines) for comparison.

Regarding the microturbulence, we employed the analytical formula for ξ in terms of $T_{\rm eff}$ and $\log g$ derived in Paper I [cf. equation (1) therein], by which ξ can be expressed as a function of $(B-V)_0$ by using the relations specific for Pleiades stars mentioned above. Such derived ξ vs. $(B-V)_0$ relation we adopted is illustrated in figure 1d (solid line), where similar relations based on alternative empirical $\xi(T_{\rm eff},\log g)$ formulas of Nissen (1981) and Edvardsson et al. (1993) are also shown for comparison (dashed lines).

The finally adopted values of $T_{\rm eff}$, $\log g$, and ξ for the program stars are given in table 2 (columns 3–5). These isochrone-based parameters are reasonably consistent with those derived spectroscopically by Funayama et al. (2009) using Fe I and Fe II lines, as can be recognized in figures 2a–2c. As to the atmospheric parameters for Procyon and the Sun, we employed the same values as used in Takeda et al. (2005b; cf. table 1 therein).

The adopted $(B-V)_0$ values, on which our parameters are based, may have inevitable ambiguities of several hundredths mag (as estimated from the dispersion of E_{B-V} in Pleiades stars shown in Fig. 4 of Breger 1986), which are translated to uncertainties in $T_{\rm eff}$ by $\sim \pm 200$ K (cf. figure 1b). Regarding errors in $\log g$ and ξ, we assume $\sim \pm 0.1$ dex and $\sim \pm 0.5$ km s^{-1} as done in Paper I, respectively, which may be reasonable estimates as judged from figures 1c and 1d.

4. Abundance determination

4.1. Spectrum-fitting analysis

The model atmosphere for each star was constructed by two-dimensionally interpolating Kurucz's (1993) ATLAS9 model grid (models with convective overshooting) with respect to $T_{\rm eff}$ and $\log g$ determined in section 3, where we exclusively applied the solar-metallicity models.

Our abundance determination procedure is basically the same as adopted in Paper I (see section 5 therein), which consists of three consecutive steps: (i) synthetic spectrum fitting to derive provisional abundances for the important elements in the relevant spectrum range, (ii) inverse calculation of the equivalent width for the line (or the blended feature) of C or O in question by using the fitting-based abundance solutions, and (iii) analysis of such established equivalent widths to derive the final abundances or abundance errors due to uncertainties in atmospheric parameters.

For the purpose of determining C and O abundances, we decided to employ C I 5380.325 line (instead of C I 7111-9 lines adopted in Paper I, which are unavailable in our data) and O I 6156–8 lines (which were also used in Paper I), since these two line features are available in all the spectra at our hand (cf. table 1). Accordingly, we selected two wavelength regions: (a) 5375–5390 Å region (comprising lines of C, Ti, Mn, and Fe), and (b) 6150–6167 Å region (comprising lines of O, Na, Si, Ca, Fe, and Ni). The atomic data of the spectral lines were taken from VALD database (Ryabchikova et al. 2015) for former 5375–5390 Å region, while from Kurucz and Bell's (1995) compilation for the latter 6150–6167 Å region (in order to maintain consistency with Paper I where the same O I 6156–8 lines were used). Although all the atomic lines contained in each database were included for each wavelength region, only the selected data for especially important lines are summarized in table 3.

As to the macroscopic broadening function (to be convolved with the intrinsic spectrum to simulate the synthetic stellar spectrum), we adopted the rotational broadening function (see, e.g., Gray 2005) with the limb-darkening coefficient of $\epsilon=0.5$, which means that $v_{\rm e}\sin i$

[4] Since there was a serious defect in Takeda et al.'s (2005a) Moon spectrum around 5375–5377 Å, we had to discard this spectrum portion in the fitting process, by which Mn abundance could not be determined for the Sun (cf. figure 3).

[5] Available at ⟨http://stev.oapd.inaf.it/cgi-bin/cmd⟩.

[6] Actually, the parameter-determination procedure described in this section was performed for two different isochrones with ages of 100 Myr and 150 Myr. Since they were found to be hardly discernible from each other in the considered $(B-V)_0$ range, we simply averaged the both results to derive the solution corresponding to 125 Myr.

(projected rotational velocity) is the control parameter for adjusting the line width in the fitting. Note here that, since neither instrumental broadening nor macroturbulence is explicitly included in our modeling, the resulting $v_{\rm e}\sin i$ solution should not always be regarded as equivalent to true (projected) rotational velocity: That is, in case of sharp lines (e.g., $\lesssim$10 km s^{-1}), our $v_{\rm e}\sin i$ solution may lead to some overestimation (though such a case is rather exceptional because rotational broadening is dominant for most of our sample stars). Accordingly, the parameters to be varied to accomplish the best fit between the theoretical and observed spectrum by using Takeda's (1995) numerical technique are (i) the abundances of relevant elements, (ii) $v_{\rm e}\sin i$, and (iii) $\Delta\lambda$ (radial velocity shift).

The convergence of the fitting solutions turned out fairly successful for most of the cases. How the theoretical spectrum for the converged solutions fits well with the observed spectrum for each of the 32 Pleiades stars (as well as Procyon and Sun/Moon) is displayed in figure 3 (5375–5390 Å fitting, where C, Ti, Mn, and Fe abundances were varied) and figure 4 (6150–6167 Å fitting, where O, Na, Si, Ca, Fe, and Ni abundances were varied). The finally resulting values of elemental abundances (A) as well as $v_{\rm e}\sin i$ derived from the fitting procedure for each region are presented in tableE.txt (on-line material).

4.2. Equivalent widths and abundance uncertainties

Next, as done in Paper I, we computed the equivalent widths for the C I 5380.325 line (W_{5380})[7] and the O I 6158 feature (W_{6158}; comprising three components) based on these fitting-based abundances. Then, the non-LTE abundances [$A^{\rm N}$(C) and $A^{\rm N}$(O)] and the relevant non-LTE corrections (Δ_{5380} and Δ_{6158}; where $\Delta \equiv A^{\rm N} - A^{\rm L}$) were derived based on these W_{5380} and W_{6158}, where the non-LTE effect for the C and O lines was taken into account as done by Takeda and Honda (2005). The resulting equivalent widths and non-LTE abundances as well as corrections for the sample stars are also given in tableE.txt (on-line material).

The uncertainties in A(C) and A(O) due to errors in the adopted atmospheric parameters were estimated by repeating the analysis on the W values while perturbing the standard parameters interchangeably by ±200 K in $T_{\rm eff}$, ±0.1 dex in $\log g$, and ±0.5 km s^{-1} in ξ (which are considered to be typical magnitudes of ambiguities; cf. the last paragraph in section 3).

We also evaluated errors due to random noises of the observed spectra by estimating S/N-related uncertainties in the equivalent width (δW) by invoking the relation derived by Cayrel (1988), $\delta W \simeq 1.6(w\delta x)^{1/2}\epsilon$, where δx is the pixel size ($\simeq$0.025 Å), w is the width of a line (which we assumed to be $\lambda v_{\rm e}\sin i/c$, where c is the velocity of light), and $\epsilon \equiv ({\rm S/N})^{-1}$. This approach is known to yield abundance errors of almost the same order of magnitude as those derived by extensive numerical simulations based on a large number of mock spectra with artificial noises (cf. Takeda & Honda 2015). We thus determined the abundances for each of the perturbed $W_+(\equiv W + \delta W)$ and $W_-(\equiv W - \delta W)$, respectively, from which the differences from the standard abundance (A) were derived as $\delta_{W+}(>0)$ and $\delta_{W-}(<0)$.

Figure 5 (C) and figure 6 (O) graphically show the resulting equivalent widths (W; with $\pm\delta W$ as error bars), non-LTE corrections (Δ), non-LTE abundances ($A^{\rm N}$; with δ_{W+} and δ_{W-} as error bars), and abundance variations in response to parameter changes ($\delta_{T\pm}$, $\delta_{g\pm}$, and $\delta_{\xi\pm}$), as functions of $T_{\rm eff}$. We can recognize from these figures that (a) non-LTE corrections are very small ($\lesssim$ a few hundredths dex) and practically negligible, (b) abundance errors due to parameter uncertainties (essentially due to ambiguities in $T_{\rm eff}$) amount to $\sim$0.1 dex for C and $\lesssim$ 0.2 dex for O (i.e., O abundances are subject to comparatively larger errors than C abundances), and (c) S/N-related abundance errors are not so significant except for $A^{\rm N}$(O) of lower-$T_{\rm eff}$ stars (6000 K $\lesssim T_{\rm eff} \lesssim$ 6500 K) where the O I line becomes appreciably weak ($W \sim$ 10 mÅ or less).

Since the present abundance study is based on a differential analysis, the results should not be significantly affected by uncertainties in line-formation or model atmospheres such as 3D hydrodynamical effect (e.g., Amarsi et al. 2016, who showed that the 3D correction for the O I 6158.2 line is on the order of $\sim$ 0.1 dex and almost $T_{\rm eff}$-independent) or treatment of convection (such as with/without overshooting, resulting in abundance differences of $\sim$ 0.1 dex; cf. Paper I) which we do not explicitly take into consideration. In particular, thanks to the fact that C and O abundances are derived from similar high-excitation lines of neutral species, the resulting [C/O] ratio (the main purpose) must be practically insensitive to such modeling details.

4.3. Differential abundances relative to the Sun

The differential abundances ([C/H], [O/H], and [Fe/H]) to be discussed in section 5 are computed as [C/H] $\equiv A^{\rm N}_{5380}$(C) − $A^{\rm N}_{5380\odot}$(C), [O/H] $\equiv A^{\rm N}_{6158}$(O) − $A^{\rm N}_{6158\odot}$(O), [Fe/H]$_{53} \equiv A^{\rm L}_{5375-90}$(Fe) − $A^{\rm L}_{5375-90\,\odot}$(Fe), and [Fe/H]$_{61} \equiv A^{\rm L}_{6150-67}$(Fe) − $A^{\rm L}_{6150-67\,\odot}$(Fe), where the adopted reference solar abundances of C, O, and Fe are $A^{\rm N}_{5380\odot}$(C) = 8.43, $A^{\rm N}_{6158\odot}$(O) = *8.81*,[8] $A^{\rm L}_{5375-90\,\odot}$(Fe) = 7.35, and

[7] Actually, several other weaker C I lines exist in the neighbourhood of this C I 5380.325 line (cf. table 3), among which the C I 5380.227 line (of higher excitation) may not be negligible. However, since W(5380.227) turned out only $\sim$ 20% compared with W(5380.325), as demonstrated in figure 5a, it can not make any important contribution. So, we considered only the C I 5380.325 line in evaluating the non-LTE correction (Δ_{5380}).

[8] Only for this O I 6158 line, we did not adopt the $A^{\rm N}$(O) solution of 8.68 derived from the 6150–6167 Å region fitting of the Moon spectrum in this study but used the value (8.81) derived in Paper I from the 6156.4–6158.6 Å fitting. This is because the strength of this O I 6158 line becomes considerably weak ($W \sim$ 2–3 mÅ) at the solar temperature and the A(O) solution resulting from fitting is appreciably sensitive to a slight difference in the vertical offset (i.e., constant C defined in Takeda 1995), which is affected by the difference in the adopted spectral range and in the treatment of 6157.4 Å feature. In the present

$A^{\rm L}_{6150-67\,\odot}$(Fe) = 7.60 (cf. tableE.txt). The results for Procyon turned out [C/H] = −0.01, [O/H] = +0.04, $[{\rm Fe/H}]_{53}$ = +0.05, and $[{\rm Fe/H}]_{61}$ = −0.07; i.e. almost equal to the solar abundances, which is consistent with the already known results (see, e.g., Sect. IVc in Takeda et al. 2008).

5. Results and discussion

5.1. Rotation and metallicity

We first examine the rotational velocity ($v_{\rm e}\sin i$) and metallicity ([Fe/H]). resulting from the fitting analysis at 5375–5390 Å and 6150–6167 Å. The $v_{\rm e}\sin i$ values derived from these two wavelength regions (ranging from $\sim$ 10 km s^{-1} to $\sim$ 110 km s^{-1}) are in good agreement with each other (figure 7a), and show a decreasing trend with a lowering of $T_{\rm eff}$ (figure 7b). While this is a trend well-known for field stars (i.e., manifest dropdown as the spectral type becomes later from F to G; see Fig. 18.21 in Gray 2005) and also seen in Hyades stars (see Fig. 15a in Paper I), the rotational velocities of Pleiades stars tend to be comparatively higher reflecting their younger ages.

Regarding the metallicity, $[{\rm Fe/H}]_{53}$ and $[{\rm Fe/H}]_{61}$ mostly agree with each other except for several stars showing appreciable deviation by $\sim$ 0.2–0.3 dex (figure 7c). A close inspection revealed that discrepancies are seen only for rapidly rotating stars ($v_{\rm e}\sin i \gtrsim 50$ km s^{-1}) while a consistency is confirmed for slower rotators of $v_{\rm e}\sin i \lesssim 50$ km s^{-1} (cf. figure 7d). According to figure 7d, $[{\rm Fe/H}]_{61}$ appears to be somewhat $v_{\rm e}\sin i$-dependent while such a trend is not seen for $[{\rm Fe/H}]_{53}$, which makes us suspect that the former is less reliable than the latter. This difference may be related to the fact that more Fe lines of appreciable strengths are available in the 5375–5390 Å region (figure 3) than in the 6150–6167 Å region (figure 4),

Accordingly, we adopted the values derived from the 5375–5390 Å region ($v_{\rm e}\sin i_{53}$ and $[{\rm Fe/H}]_{53}$) as the final results in table 2. Figures 2d ($v_{\rm e}\sin i$) and 2e ([Fe/H]) show the comparison of these with Funayama et al.'s (2009) results, where we can see a fairly good agreement for $v_{\rm e}\sin i$ while some (though not so serious) discrepancy up to $\lesssim$ 0.2 dex is seen for [Fe/H].

5.2. C and O abundances

We now discuss the trends of C and O abundances as well as C/O ratios of the Pleiades stars. The finally resulting values of [Fe/H], [C/H], [O/H], and [C/O] for the 32 program stars are plotted against $T_{\rm eff}$ in figure 8, where combined uncertainties due to parameter ambiguities and data noises (cf. subsection 4.2) are shown by error bars. The following characteristics are read from these figures:

— No systematic dependence upon $T_{\rm eff}$ is observed in these results and thus almost homogeneous.

— However, while [Fe/H] appears to be nearly solar, we can see a trend of subsolar [C/H] (< 0) and supersolar [O/H] (> 0), resulting in a manifest tendency of subsolar [C/O] < 0.

— This can be quantitatively confirmed. Since abundances from rapid rotators tend to be less reliable (as seen for the case of $[{\rm Fe/H}]_{61}$ in subsection 5.1), we confine ourselves only to sharp-line stars of $v_{\rm e}\sin i < 50$ km s^{-1} (filled symbols in figure 8). Then, we have $\langle[{\rm Fe/H}]\rangle = 0.00$ ($\sigma = 0.08$), $\langle[{\rm C/H}]\rangle = -0.12$ ($\sigma = 0.06$), $\langle[{\rm O/H}]\rangle = +0.08$ ($\sigma = 0.16$), and $\langle[{\rm C/O}]\rangle = -0.20$ ($\sigma = 0.14$), which further result in the Fe-scaled abundance ratios of $\langle[{\rm C/Fe}]\rangle = -0.12$ ($\sigma = 0.10$) and $\langle[{\rm O/Fe}]\rangle = +0.08$ ($\sigma = 0.21$).

Consequently, regarding the C and O abundances of Pleiades F–G stars relative to the Sun, we conclude that [C/H] is underabundant by ~ -0.1 dex, [O/H] is overabundant by $\sim +0.1$ dex, and thus [C/O] is underabundant by ~ -0.2 dex, each holding with a dispersion of $\lesssim$ 0.1–0.2 dex.

5.3. [C/O] ratio of the Pleiades cluster and its implication

We thus found that [C/O] in the Pleiades cluster is apparently subsolar by ~ -0.2 dex as a result of subsolar C and supersolar O. This means that the trend of negative [C/O] suspected in Hyades stars ([C/O] ~ -0.1 dex; cf. Sect. 6.2 in Paper I) is more accentuated in Pleiades stars, which makes contrast with the case of field solar-type stars of near-solar metallicity ([Fe/H] $\sim$ 0) where [C/O] $\sim$ 0 holds on the average (cf. Fig. 6 in Takeda & Honda 2005). In order to clarify this fact, we recalculated the average values of $\langle[{\rm Fe/H}]\rangle$, $\langle[{\rm C/Fe}]\rangle$, $\langle[{\rm O/Fe}]\rangle$, and $\langle[{\rm C/O}]\rangle$ for Hyades stars (here, only those with $T_{\rm eff} > 5800$ K were used to make the sample as similar as possible)[9] as we have done for the Pleiades stars in subsection 5.2. These mean abundances obtained for both Hyades and Pleiades are plotted by large symbols in figure 9, where the corresponding values of field stars (the results were derived by using C I 5380 and O I 6158 lines while restricting to only F–G stars of $T_{\rm eff} > 5800$ K) are also shown. We can confirm by inspecting figure 9c that the $\langle[{\rm C/O}]\rangle$ values for Hyades and Pleiades stars locate at the lower envelope of the [C/O] vs. [Fe/H] distribution of field stars, which suggests that the C/O ratios of these two open clusters rather deviate from the mean trend exhibited by the latter. Why do the C/O ratios of cluster stars ([C/O] ~ -0.2 to -0.1) are so different from those of F–G stars (of near-solar metallicity) and the Sun ([C/O] $\sim$ 0)? Does it have anything to do with the clear distinction in stellar ages between the former ($\sim$ 120–130 Myr for Pleiades and $\sim$ 625 Myr for Hyades; cf. section 1) and the latter ($\sim$ 1–10 Gyr; cf. Fig. 14 of Takeda 2007) ?

Here, it is important to note that the result we derived for Pleiades F–G stars is quite similar to that recently reported for B-type stars. That is, Nieva and Przybilla (2012) determined the light-element abundances for 20 B-

case, solution from the fitting in the narrower wavelength region as done in Paper I is more reliable than that from the wider-region fitting such as adopted in this study. See appendix 1, where the reasoning of this choice is described in more detail.

[9] The mean results for Hyades stars with $T_{\rm eff} > 5800$ K are: $\langle[{\rm Fe/H}]\rangle = +0.06$ ($\sigma = 0.10$), $\langle[{\rm C/H}]\rangle = +0.12$ ($\sigma = 0.09$), $\langle[{\rm O/H}]\rangle = +0.21$ ($\sigma = 0.20$), and $\langle[{\rm C/O}]\rangle = -0.08$ ($\sigma = 0.19$). Accordingly, [X/Fe] ratios for Hyades are $\langle[{\rm C/Fe}]\rangle = +0.06$ ($\sigma = 0.09$) and $\langle[{\rm O/Fe}]\rangle = +0.14$ ($\sigma = 0.23$).

type stars (16000 K $\lesssim T_{\rm eff} \lesssim$ 33000 K, $6M_\odot \lesssim M \lesssim 19M_\odot$) and concluded that the mean C and O abundances relative to Asplund et al.'s (2009) solar abundances are $\langle$[C/H]$\rangle = -0.10$ and $\langle$[O/H]$\rangle = +0.07$ (see Table 9 or Fig. 12 of their paper); i.e., subsolar [C/H] as well as supersolar [O/H] by ~ 0.1 dex, resulting in [C/O] ~ -0.2 dex, which is just as we have obtained for the Pleiades stars. Considering that these B-type stars around $M \sim 10M_\odot$ have typical ages of several tens Myr (e.g., Georgy et al. 2013), this result of subsolar [C/O] appears to be the common characteristics seen for young stars born within $\lesssim 10^8$ yr.

Therefore, the same discussion as developed by Nieva and Przybilla (2012) regarding the Sun and B-type stars may hold for the present case. Their important suggestion was that the Sun was born in comparatively inner/metal-rich region at the galactocentric radius of $R_{\rm G} \sim$ 5–6 kpc and has migrated outward to the current position of $R_{\rm G} \sim 8$ kpc, which naturally explains the paradox why the light-element abundances of such young stars are nearly the same (or even slightly underabundant) compared to the Sun (age of 4.6×10^9 yr) despite that chemical evolution must have enriched the Galactic gas during the passage of time. As they pointed out, this hypothesis leads to a reasonable account for the larger C-to-O abundance ratio of the Sun compared to those of young stars in the solar neighborhood, because C/O in the Galactic disk tends to decline with an increase of $R_{\rm G}$ as indicated from recombination-line observations of H II regions (Esteban et al. 2005) and supported by some theoretical models of chemical evolution (Carigi et al. 2005).

Consequently, according to this scenario, our observational fact that the [C/O] values in the Pleiades F–G stars are by ~ -0.2 dex lower than the Sun may be interpreted as due to the difference of C/O ratios in two kinds of interstellar gases: (1) which recently formed young stars near to the current Sun ($R_{\rm G} \sim 8$ kpc, age of $\lesssim 10^8$ yr) and (2) which formed the Sun in the inner region ($R_{\rm G} \sim$ 5–6 kpc) long before (4.6×10^9 yr ago). We should remark, however, that the [C/O] values of field stars of near-solar metallicity ([Fe/H] ~ 0) studied by Takeda and Honda (2005) evenly distribute around ~ 0 (figure 9c), which means that the Sun is not exceptional compared to nearby solar-type stars in terms of the C/O ratio. So, if our Sun really has significatly changed its orbit since its birth, such a migration may not necessarily be a rare phenomenon for stars in the Galactic disk.

In summary, while we found based on our C and O abundance study of 32 Pleiades stars that the [C/O] ratios of these recently formed young stars are by ~ -0.2 dex lower than those of the Sun and similarly aged solar-metalicity field stars, this difference between these two age groups is presumably due to (not the direct time-evolution effect but) the orbit migration mechanism which Galactic stars may undergo in a long time. Given this scenario, detecting C-rich stars with N(C)/N(O)$>$ 0.8 (mentioned in section 1) would be hardly possible among young stars in the solar neighborhood, while such a possibility may be higher for old metal-rich stars which were born near to the Galactic bulge.

Special thanks are due to H. Funayama for his substantial contribution in obtaining the observational data for 25 Pleiades stars in the 2006–2007 season, upon which this study heavily depends.

This research has made use of the SIMBAD database (operated by CDS, Strasbourg, France) as well as the VALD database (operated at Uppsala University, the Institute of Astronomy RAS in Moscow, and the University of Vienna).

Data reduction was in part carried out by using the common-use data analysis computer system at the Astronomy Data Center (ADC) of the National Astronomical Observatory of Japan.

Appendix 1. Solar oxygen abundance derived from the O I 6156–8 lines

In deriving differential [O/H] (subsection 4.3), we intentionally adopted $A_\odot$(O) = 8.81 derived by Takeda and Honda (2005) as the reference solar oxygen abundance, instead of the slightly lower value of 8.68 obtained in this study, since we believe that the former is more reliable than the latter. This is related to the difficulty involved with O-abundance determination from O I 6156–8 lines in the spectrum of the Sun, where lines of other species are blended because of its comparatively low $T_{\rm eff}$. Actually, there are differences between these two analyses, although they used the same model atmosphere and the same Moon spectrum.

— First, Takeda and Honda (2005) carried out the fitting in the limited 6156.4–6158.6 Å region (only 2.2 Å wide) while we applied fittings to a much wider 6150–6167 Å region in this study since stars with considerably broad lines (up to $v_{\rm e} \sin i \sim 100$ km s^{-1}) are involved (i.e., to ensure the stability of solutions).

— Second, although both studies were based on the same Kurucz and Bell's (1995) compilation for the atomic line data, Takeda and Honda (2005) applied arbitrary chages in the gf values of 4 Ti lines (cf. footnote 5 therein) in order to reproduce the absorption feature at $\sim$ 6157.4 Å, while such modifications were not applied in this study where all the data given in Kurucz and Bell (1995) were employed without any change since such a $\sim$ 6157.4 Å feature is seen only for lower-$T_{\rm eff}$ stars ($T_{\rm eff} \lesssim 6000$ K; cf. Fig. 1 in Takeda & Honda 2005) and irrelevant for most of our sample stars.

The resulting $A_\odot$(O) solutions for these two cases show a difference by 0.13 dex (8.81 and 8.68) because of the different wavelength span and different treatment for the $\sim$ 6157.4 Å feature (figure 10a). However, we have a good reason to believe that the former solution (8.81) is more reliable than the latter (8.68), as manifested from the simulated strength of the strongest 6158.2 Å line (which is considered to be practically blend-free and most reliable among the three O I features, in contrast to those at 6156.0 and 6156.8 Å being appreciably contaminated by lines of other species) in comparison with Kurucz et al.'s (1984) solar flux spectrum of very high resolving power (figure 10b). (Besides, if we adopt 8.68, we have

$[O/H]_{Procyon} = +0.17$, which is unacceptably too high for this star known to have near-solar composition.[10]) It should also be remarked that a consistency is accomplished by this choice of using Takeda and Honda's (2005) $A_\odot(O) = 8.81$ with regard to the comparison of figure 9, where the mean values of [O/Fe] and [C/O] for the Pleiades stars are compared with those of field F–G stars derived in Takeda and Honda (2005).

Regarding the lines of other species contaminating the relevant O I lines in the solar spectrum, the weakest O I 6156.0 Å line is severely blended with the Ca I 6156.023 line which we took into consideration (cf. table 3). Meanwhile, the O I 6156.8 line (medium strength) is evidently blended with some other line (cf. figure 10b) which is not included in Kurucz and Bell's (1995) compilation. This unknown blend may be due to Fe I, since the VALD database contains Fe I 6156.804 (χ_{low} = 4.956 eV, $\log gf = -1.495$), though this $\log gf$ must be erroneously too large as it predicts too strong contribution [$W_\odot \sim 13$ mÅ for $A_\odot$(Fe) = 7.50] compared to the required amount of only ~ 2 mÅ. Finally, although Pereira, Asplund, and Kiselman (2009) suspected that the strongest O I 6158.2 line is blended by weak CN lines, this effect (if any exists) would not be so significant, because Bertran de Lis et al. (2015) reported that the oxygen abundances derived from O I 6158.2 and [O I] 6300.30 lines agree well with each other. In any event, as the strengths of such Fe I as well as CN lines progressively decrease with an increase in $T_{\rm eff}$, their blending effect is negligible for most of our Pleiades stars which have $T_{\rm eff} \gtrsim 6000$ K.

Appendix 2. Lithium abundances of 7 Pleiades stars

We originally wished to organize this study on Pleiades stars in close analogy with Paper I, where not only C and O abundances but also Li abundances of Hyades F–G stars were determined. Unfortunately, given that we primarily relied on the available archived data for many of our sample stars (25 out of 32), Li abundances for those stars could not be derived as the Li I 6708 line was outside the wavelength range of their spectra (cf. table 1). Yet, since this Li line was included in the spectra of 7 stars (i.e., No. 26–32 in table 1) newly observed by ourselves in the 2015–2016 season, we could determine their Li abundances, which we briefly report here for reference.

The procedure for Li abundance determination is essentially the same as described in Takeda and Kawanomoto (2005) (also adopted in Paper I), which may be consulted for more details. The best-fit theoretical spectrum with the observed data in the 6702–6712 Å region is shown in figure 10 for each star. The resulting equivalent width of the Li I 6708 doublet (in mÅ), non-LTE abundance (in the usual normalization of A(H)=12), and non-LTE correction (in dex) are (W, $A^{\rm N}$(Li), Δ) = (81.3, 3.07, 0.00), (168.2, 3.50, +0.07), (137.7, 3.10, +0.10), (142.5, 3.34, +0.05), (55.6, 3.00, −0.03), (144.4, 3.30, +0.06), and (123.6, 3.24, +0.04), for HD 23269 (No. 26), HD 23386 (No. 27), MSK 65 (No. 28), BD +22 548 (No. 29), HD 23513 (No. 30), HD 282967 (No. 31), and HD 283067 (No. 32), respectively.

If these $A^{\rm N}$(Li) values of 7 stars (ranging at 5800 K $\lesssim T_{\rm eff} \lesssim$ 6600 K, overlapping the Hyades Li-dip of $T_{\rm eff} \sim$ 6200–6800 K) are overplotted on the $A^{\rm N}$(Li) vs. $T_{\rm eff}$ relation of Hyades stars presented in Fig. 14e of Paper I, we can confirm that the primordial Li abundance (~ 3.3) is nearly preserved in the photosphere of Pleiades stars at $T_{\rm eff} \sim$ 5800–6600 K with little sign of depletion, in marked contrast with the case of Hyades stars at the Li chasm. This is consistent with the results of previous studies (see, e.g., Fig. 1 of Boesgaard, Armengaud, & King 2003).

[10] The oxygen abundance of Procyon (= HR 2943 = HD 61421 = HIP 37279) relative to the Sun has already been determined in several published studies using various lines of different reliability. For example, according to Steffen's (1985) analysis, $[O/H]_{Procyon}$ is −0.17 (from O I 6156.8; unreliable because of the blending in the solar spectrum as mentioned above), −0.01 (from O I 6158.2; most credible), and −0.05 ([O I] 6300.3). Edvardsson et al. (1993) derived $[O/H]_{Procyon} = -0.05$ (O I 6158.2, O I 7771–5), while $[O/H]_{Procyon} = +0.02$ (from [O I] 6300, O I 7771–5) was reported in Allende Prieto et al.'s (2004) S^{4}N project summarized at ⟨http://hebe.as.utexas.edu/s4n/⟩. Further, Takeda and Honda (2005) derived $[O/H]_{Procyon} = -0.04$ (from [O I] 6300), +0.06 (from O I 6157–8; finally adopted by them), and +0.07 (from O I 7771–5). These results indicate that the photospheric O abundances of Procyon and Sun are quite similar to a degree of several hundredths dex.

References

Allende Prieto, C., Barklem, P. S., Lambert, D. L., & Cunha, K. 2004, A&A, 420, 183

Amarsi, A. M., Asplund, M., Collet, R., & Leenaarts, J. 2016, MNRAS, 455, 3735

Asplund, M., Grevesse, N., Sauval, A. J., & Scott, P. 2009, ARA&A, 47, 481

Basri, G., Marcy, G. W., & Graham, J. R. 1996, ApJ, 458, 600

Bertran de Lis, S., Delgado Mena, E., Adibekyan, V. Kh, Santos, N. C., & Sousa, S. G. 2015, A&A, 576, A89

Boesgaard, A. M. 2005, in Cosmic Abundances as Records of Stellar Evolution and Nucleosynthesis in honor of David L. Lambert, eds. T. G. Barnes III and F. N. Bash, ASP Conf. Ser., Vol. 336, p.39 (San Francisco, ASP)

Boesgaard, A. M., Armengaud, E., & King, J. R. 2003, ApJ, 582, 410

Bonatto, Ch, Bica, E., & Girardi, L. 2004, A&A, 415, 571

Bond, J. C., O'Brien, D. P., & Lauretta, D. S. 2010, ApJ, 715, 1050

Breger, M. 1986, ApJ, 309, 311

Bressan, A., Marigo, P., Girardi, L., Salasnich, B., Dal Cero, C., Rubele, S., Nanni, A. 2012, MNRAS, 427, 127

Bressan, A., Marigo, P., Girardi, L., Nanni, A., & Rubele, S. 2013, EPJ Web of Conferences, 43, 3001 (DOI: http://dx.doi.org/10.1051/epjconf/20134303001)

Carigi, L., Peimbert, M., Esteban, C., & García-Rojas, J. 2005, ApJ, 623, 213

Cayrel, R. 1988, in The Impact of Very High S/N Spectroscopy on Stellar Physics, Proc. IAU Symp. 132, eds. G. Cayrel de Strobel & M. Spite (IAU), p. 345

Delgado Mena, E., Israelian, G., Gonzáles Hernández, J. I., Bond, J. C., Santos, N. C., Udry, S., & Mayor, M. 2010, ApJ, 725, 2349

Edvardsson, B., Andersen, J., Gustafsson, B., Lambert, D. L., Nissen, P. E., & Tomkin, J. 1993, A&A, 275, 101
Esteban, C., García-Rojas, J., Peimbert, M., Peimbert, A., Ruiz, M. T., Rodríguez, M., & Carigi, L. 2005, ApJ, 618, L95
Friel, E. D., & Boesgaard, A. M. 1990, ApJ, 351, 480
Funayama, H., Itoh, Y., Oasa, Y., Toyota, E., Hashimoto, O., & Mukai, T. 2009, PASJ, 61, 931
Gebran, M., & Monier, R. 2008, A&A, 483, 567
Georgy, C., Ekström, S., Granada, A., Meynet, G., Mowlavi, N., Eggenberger, P., & Maeder, A. 2013, A&A, 553, A24
Gray, D. F. 2005, The Observation and Analysis of Stellar Photospheres, 3rd ed. (Cambridge: Cambridge University Press)
Gustafsson, B., Karlsson, T., Olsson, E., Edvardsson, B., & Ryde, N. 1999, A&A, 342, 426
Hertzsprung, E. 1947, Annalen van de Sterrewacht te Leiden, 19, A1
Kurucz, R. L. 1993, Kurucz CD-ROM, No. 13 (Harvard-Smithsonian Center for Astrophysics)
Kurucz, R. L., & Bell, B. 1995, Kurucz CD-ROM, No. 23 (Harvard-Smithsonian Center for Astrophysics)
Kurucz, R. L., Furenlid, L., Brault, J., & Testerman, L. 1984, Solar Flux Atlas from 296 to 1300 nm (Sunspot, New Mexico: National Solar Observatory)
Leushin, V. V., & Topil'skaya, G. P. 1987, Astrophysics, 25, 415
Melis, C., Reid, M. J., Mioduszewski, A. J., Stauffer, J. R., & Bower, G. C. 2014, Science, 340, 1029
Nakajima, T., & Sorahana, S.2016, ApJ, in press (arXiv: 1607.07528)
Nieva, M.-F., & Przybilla, N. 2012, A&A, 539, A143
Nissen, P. E. 1981, A&A, 97, 145
Nissen, P. E., Chen, Y. Q., Carigi, L., Schuster, W. J., & Zhao, G. 2014, A&A, 568, A25
Pereira, T. M. D., Asplund, M., & Kiselman, D. 2009, A&A, 508, 1403
Perryman, M. A. C., et al. 1998, A&A, 331, 81
Petigura, E. A., & Marcy, G. W. 2011, ApJ, 735, 41
Ryabchikova, T., Piskunov, N., Kurucz, R. L., Stempels, H. C., Heiter, U., Pakhomov, Yu, & Barklem, P. S. 2015, Physica Scripta, Vol. 90, Issue 5
Steffen, M. 1985, A&AS, 59, 403
Takeda, Y. 1995, PASJ, 47, 287
Takeda, Y. 2007, PASJ, 59, 335
Takeda, Y., et al. 2005a, PASJ, 57, 13
Takeda, Y., Han, I., Kang, D.-I., Lee, B.-C., & Kim, K.-M. 2008, JKAS, 41, 83
Takeda, Y., & Honda, S. 2005, PASJ, 57, 65
Takeda, Y., & Honda, S. 2015, PASJ, 67, 25
Takeda, Y., Honda, S., Ohnishi, T., Ohkubo, M, Hirata, R., & Sadakane, K. 2013, PASJ, 65, 53 (Paper I)
Takeda, Y., & Kawanomoto, S. 2005, PASJ, 57, 45
Takeda, Y., Ohkubo, M., Sato, B., Kambe, E., & Sadakane, K. 2005b, PASJ, 57, 27 [Erratum: PASJ, 57, 415]

Table 1. Basic observational data of the program stars.

No.	Star	HII#	V	$B-V$	Instr.	$t_{\rm exp}^{\rm total}$	S/N	Obs. date
(1)	(2)	(3)	(4)	(5)	(6)	(7)	(8)	(9)
1	V1038 Tau	314	10.66	0.66	G1	420	60	2007 Jan 13, 14, 15
2	HD 23289	470	8.86	0.40	G1	81	120	2006 Jan 25
3	MSK 39	489	10.41	0.63	G1	510	80	2006 Jan 30, 2007 Jan 11, 12
4	HD 23325	531	8.58	0.34	H	65	150	2006 Jan 11
5	HD 23375	697	8.59	0.35	G1	30	40	2007 Jan 15
6	V855 Tau	727	9.71	0.56	G1	44	60	2006 Jan 25
7	HD 23585	1284	8.37	0.29	H	30	150	2006 Jan 11
8	HD 23584	1309	9.46	0.47	H	90	100	2006 Jan 15
9	HD 282972	1794	10.36	0.66	G1	180	70	2006 Jan 28
10	BD +23 551	1797	10.13	0.56	G1	132	100	2006 Jan 27
11	BD +22 574	2506	10.27	0.60	G1	190	100	2006 Jan 29
12	HD 24194	3179	10.05	0.57	H	240	120	2006 Dec 6
13	BD +23 472	3301	9.54	0.51	H	30	40	2006 Dec 10
14	HD 22887	3309	9.18	0.45	H	60	80	2006 Jan 12
15	HD 22977	3310	9.11	0.47	H	90	120	2006 Jan 12, Dec 10
16	HD 23312	3314	9.49	0.49	H	180	130	2006 Jan 12, 15
17	HD 23488	3319	8.73	0.37	H	75	150	2006 Jan 11
18	HD 23975	3326/5026	9.64	0.52	H	150	160	2006 Dec 10
19	BD +21 503	⋯	10.35	0.62	G1	480	70	2007 Jan 10, 11
20	BD +22 521	⋯	10.07	0.54	H	240	80	2006 Dec 11. 12
21	BD +23 486	⋯	10.34	0.60	G1	300	80	2007 Jan 15, 18
22	BD +25 591	⋯	10.06	0.56	H	180	100	2006 Dec 10
23	BD +25 610	3442	9.99	0.59	G1	360	90	2007 Jan 9, 10
24	HD 23598	⋯	9.83	0.54	H	60	50	2006 Dec 6
25	HD 24655	3332	9.07	0.45	H	85	100	2006 Jan 12, Dec 9
26	HD 23269	405	9.84	0.54	G2	360	120	2016 Jan 14
27	HD 23386	739	9.57	0.62	G2	180	100	2015 Dec 18
28	MSK 65	761	10.56	0.71	G2	300	120	2016 Mar 16, 22, 24, 25
29	BD +22 548	923	10.16	0.61	G2	270	110	2016 Feb 2
30	HD 23513	1139	9.37	0.48	G2	240	150	2015 Nov 30
31	HD 282967	1514	10.48	0.64	G2	360	90	2016 Feb 15
32	HD 283067	2786	10.31	0.60	G2	300	110	2016 Mar 1, 15

(1) Object number (arbitrarily assigned). (2) Star name. (3) Hertzsprung's (1947) HII number. (4) Observed V magnitude. (5) Observed $B-V$ color. (6) Key to the used instrument (G1 ⋯ GAOES data in 2006–2007 covering 4870–6670 Å, G2 ⋯ GAOES data in 2015–2016 covering 4950–6800 Å, H ⋯ HIDES data in 2006 covering 5340–6580 Å). (7) Total exposure time (in minutes). (8) Signal-to-noise ratio directly measured around $\sim$ 5370–5390 Å. (9) Dates of observations.

Table 2. Stellar parameters and the results of abundance analysis.

No.	Object	$T_{\rm eff}$	$\log g$	ξ	$v_{\rm e}\sin i$	[Fe/H]	$W^{\rm C}_{5380}$	$\Delta^{\rm C}_{5380}$	[C/H]	$W^{\rm O}_{6158}$	$\Delta^{\rm O}_{6158}$	[O/H]
(1)	(2)	(3)	(4)	(5)	(6)	(7)	(8)	(9)	(10)	(11)	(12)	(13)
1	V1038 Tau	5982	4.50	1.2	36	+0.09	21.2	−0.01	−0.03	9.9	0.00	+0.32
2	HD 23289	6945	4.32	2.2	27	+0.05	37.9	−0.02	−0.14	20.5	−0.02	−0.05
3	MSK 39	6067	4.48	1.2	18	+0.01	23.6	−0.01	−0.02	8.1	0.00	+0.14
4	HD 23325	7289	4.31	2.5	78	+0.27	31.3	−0.02	−0.35	35.6	−0.04	+0.04
5	HD 23375	7227	4.31	2.5	87	−0.02	30.9	−0.02	−0.34	54.2	−0.04	+0.35
6	V855 Tau	6266	4.44	1.5	51	+0.01	21.1	−0.01	−0.19	7.3	0.00	−0.07
7	HD 23585	7629	4.31	2.9	110	+0.22	54.6	−0.02	−0.10	50.4	−0.05	+0.01
8	HD 23584	6612	4.37	1.8	78	−0.10	30.3	−0.01	−0.15	21.2	−0.01	+0.22
9	HD 282972	5982	4.50	1.2	14	+0.04	18.3	−0.01	−0.11	4.2	0.00	−0.11
10	BD +23 551	6266	4.44	1.5	21	−0.02	21.7	−0.01	−0.17	8.7	0.00	+0.02
11	BD +22 574	6150	4.46	1.3	15	+0.01	23.9	−0.01	−0.06	9.0	0.00	+0.13
12	HD 24194	6235	4.45	1.4	8	−0.01	23.0	−0.01	−0.12	9.2	0.00	+0.07
13	BD +23 472	6446	4.40	1.7	43	−0.09	27.7	−0.01	−0.12	15.2	0.00	+0.16
14	HD 22887	6700	4.35	1.9	92	−0.14	31.3	−0.02	−0.17	25.5	−0.01	+0.26
15	HD 22977	6612	4.37	1.8	57	+0.04	41.0	−0.02	+0.05	22.2	−0.01	+0.25
16	HD 23312	6527	4.38	1.7	12	−0.14	30.5	−0.01	−0.10	17.4	0.00	+0.17
17	HD 23488	7108	4.31	2.3	19	−0.06	40.3	−0.02	−0.15	31.7	−0.03	+0.09
18	HD 23975	6407	4.41	1.6	23	−0.17	29.6	−0.01	−0.06	14.7	0.00	+0.17
19	BD +21 503	6095	4.48	1.3	33	−0.09	22.5	−0.01	−0.06	17.0	0.00	+0.53
20	BD +22 521	6333	4.42	1.5	27	+0.16	26.0	−0.01	−0.11	7.8	0.00	−0.10
21	BD +23 486	6150	4.46	1.3	12	+0.03	21.6	−0.01	−0.12	9.6	0.00	+0.16
22	BD +25 591	6266	4.44	1.5	35	+0.02	22.9	−0.01	−0.14	13.1	0.00	+0.23
23	BD +25 610	6178	4.46	1.4	10	−0.08	20.4	−0.01	−0.16	8.9	0.00	+0.10
24	HD 23598	6333	4.42	1.5	69	+0.03	31.6	−0.01	+0.01	35.9	0.00	+0.79
25	HD 24655	6700	4.35	1.9	25	−0.01	38.4	−0.02	−0.04	18.7	−0.01	+0.08
26	HD 23269	6333	4.42	1.5	19	+0.07	26.8	−0.01	−0.09	9.2	0.00	−0.01
27	HD 23386	6095	4.48	1.3	15	+0.08	19.9	−0.01	−0.13	5.5	0.00	−0.07
28	MSK 65	5826	4.53	1.0	13	−0.11	12.3	−0.01	−0.24	2.6	0.00	−0.21
29	BD +22 548	6123	4.47	1.3	19	+0.12	18.8	−0.01	−0.18	4.6	0.00	−0.18
30	HD 23513	6569	4.37	1.8	33	+0.01	36.7	−0.02	−0.01	18.8	−0.01	+0.18
31	HD 282967	6039	4.49	1.2	16	+0.05	16.0	−0.01	−0.22	6.3	0.00	+0.04
32	HD 283067	6150	4.46	1.3	25	+0.02	17.9	−0.01	−0.22	8.4	0.00	+0.09

(1) Object number. (2) Star name. (3) Effective temperature (in K). (4) logarithm of surface gravity (in cm s^{-2}). (5) Microturbulence (in km s^{-1}). (6) Projected rotational velocity (in km s^{-1}) derived from 5375–5390 Å fitting. (7) Fe abundance (LTE) relative to the Sun (in dex) derived from 5375–5390 Å fitting. (8) Equivalent width (in mÅ) for C I 5380.325. (9) Non-LTE correction for C I 5380.325 (in dex). (10) Non-LTE carbon abundance relative to the Sun (in dex). (11) Equivalent width (in mÅ) for O I 6158 comprising 3 components. (9) Non-LTE correction for O I 6158 (in dex). (10) Non-LTE oxygen abundance relative to the Sun (in dex). See subsection 4.3 for more details regarding the derivation of [Fe/H], [C/H], and [O/H].

Table 3. Atomic parameters of important lines relevant for spectrum fitting.

Species (1)	λ (2)	χ (3)	$\log gf$ (4)	Gammar (5)	Gammas (6)	Gammaw (7)	Remark (8)
			[5375–5390 Å fitting]				
Mn I	5377.607	3.844	−0.166	7.90	−5.39	−7.59	
C I	5378.910	8.851	−0.912	8.34	−1.52	−6.59	minor contribution
Fe I	5379.573	3.695	−1.514	7.85	−6.13	−7.58	
C I	5380.227	8.851	−1.066	8.11	−1.86	−6.58	minor contribution
C I	5380.267	8.851	−2.096	7.99	−1.96	−6.62	negligible
C I	5380.325	7.685	−1.616	8.69	−5.65	−7.37	C 5380: most important
Ti II	5381.022	1.566	−1.970	8.15	−6.59	−7.85	
Fe I	5382.263	5.669	−0.252	8.33	−4.39	−7.39	
Fe I	5383.368	4.312	+0.645	8.30	−5.01	−7.22	
Fe I	5386.333	4.154	−1.770	8.45	−4.47	−7.17	
Fe I	5387.480	4.143	−2.034	8.10	−5.66	−7.70	
C I	5388.226	8.847	−1.183	8.34	−2.05	−6.66	minor contribution
Fe I	5389.478	4.415	−0.410	8.32	−4.81	−7.16	
			[6150–6167 Å fitting]				
Fe I	6151.617	2.176	−3.299	8.19	−6.20	−7.82	
Na I	6154.226	2.102	−1.560	7.85	−4.39	(−7.29)	
Si I	6155.134	5.619	−0.400	(7.77)	(−4.45)	(−7.05)	
Si I	6155.693	5.619	−1.690	(7.77)	(−4.45)	(−7.05)	
O I	6155.961	10.740	−1.401	7.60	−3.96	(−7.23)	O 6156
O I	6155.971	10.740	−1.051	7.61	−3.96	(−7.23)	O 6156
O I	6155.989	10.740	−1.161	7.61	−3.96	(−7.23)	O 6156
Ca I	6156.023	2.521	−2.200	7.49	−4.69	−7.50	
O I	6156.737	10.740	−1.521	7.61	−3.96	(−7.23)	O 6157
O I	6156.755	10.740	−0.931	7.61	−3.96	(−7.23)	O 6157
O I	6156.778	10.740	−0.731	7.62	−3.96	(−7.23)	O 6157
Fe I	6157.725	4.076	−1.260	7.70	−6.06	−7.84	
O I	6158.149	10.741	−1.891	7.62	−3.96	(−7.23)	O 6158
O I	6158.172	10.741	−1.031	7.62	−3.96	(−7.23)	O 6158
O I	6158.187	10.741	−0.441	7.61	−3.96	(−7.23)	O 6158
Na I	6160.747	2.104	−1.260	7.85	−4.39	(−7.29)	
Ca I	6161.297	2.523	−1.020	7.49	−4.69	−7.50	
Ca I	6162.173	1.899	+0.100	7.82	−5.07	−7.59	
Ni I	6163.418	4.105	−0.682	8.31	−4.06	−7.76	
Ca I	6163.755	2.521	−1.020	7.48	−4.69	−7.50	
Fe I	6165.361	4.143	−1.550	7.94	−6.16	−7.83	
Ca I	6166.439	2.521	−0.900	7.48	−4.69	−7.50	

(1) Line species. (2) Air wavelength (in Å). (3) Lower excitation potential (in eV). (4) Logarithm of g_i (statistical weight of the lower level) times f_{ij} (absorption oscillator strength). (5) Logarithm of the radiation damping width in unit of s^{-1} [$\log\gamma_{\rm rad}$] (6) Logarithm of the Stark damping width (s^{-1}) per electron density (cm^{-3}) at 10^4 K [$\log(\gamma_{\rm e}/N_{\rm e})$]. (7) Logarithm of the van der Waals damping width (s^{-1}) per hydrogen density (cm^{-3}) at 10^4 K [$\log(\gamma_{\rm w}/N_{\rm H})$]. (8) Miscellaneous remarks. The data in the 5375–5390 Å region were adopted from the VALD database, while those in the 6150–6167 Å region were taken from the compilation of Kurucz and Bell (1995) in order to maintain consistency with Paper I. Parenthesized values of the damping parameters are those computed according to the default treatment of Kurucz's (1993) WIDTH9 program (cf. Leusin, Topil'skaya 1987), since they are not given in the original database.

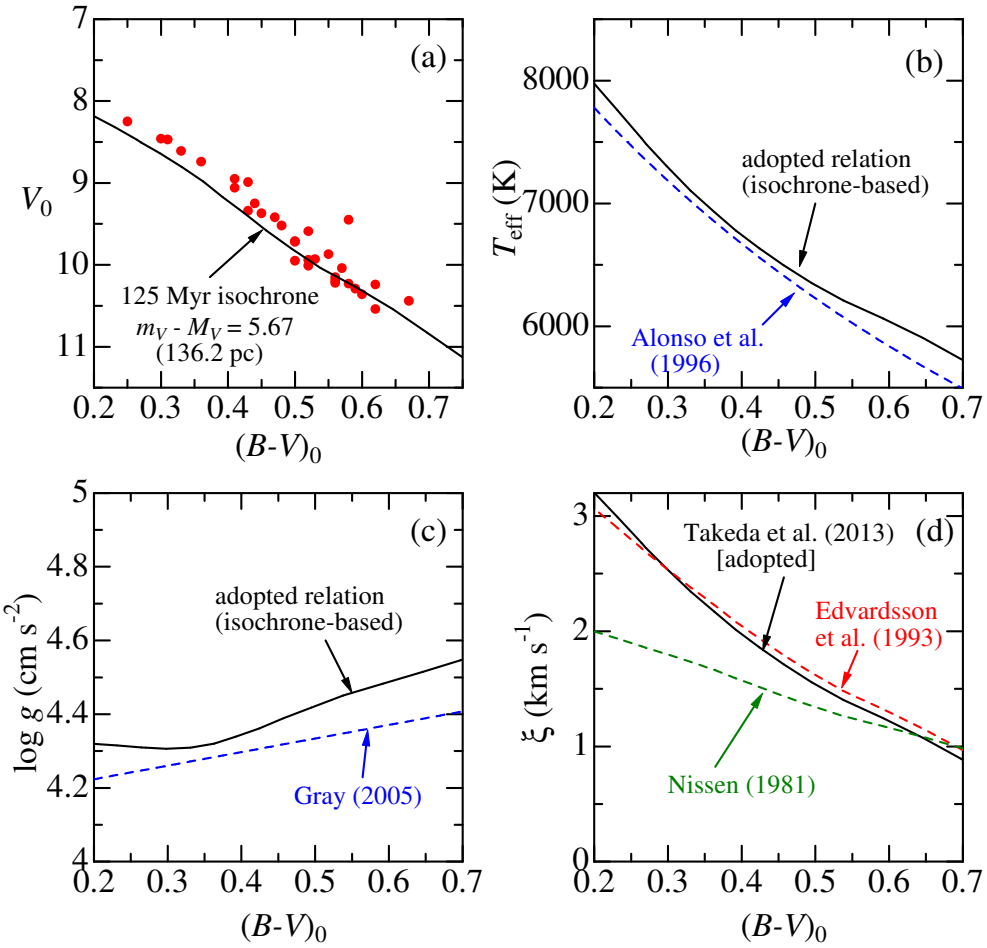

Fig. 1. (a) Solid lines: Theoretical PARSEC isochrone (Bressan et al. 2012, 2013) of solar-metallicity corresponding to the age of 125 Myr, which was converted from the absolute to apparent magnitude scale by using the Pleiades distance of 136.2 pc (Melis et al. 2014). Symbols: V_0 vs. $(B-V)_0$ diagram of the program stars, where the interstellar reddening effect was corrected by assuming $E_{B-V} = A_V/3.1 = 0.03$. (b) Isochrone-based $T_{\rm eff}$ vs. $(B-V)_0$ relation adopted for the Pleiades stars (solid line) compared with Alonso et al.'s (1996) empirical calibration for the case of [Fe/H] = 0 (dashed line). (c) Isochrone-based $\log g$ vs. $(B-V)_0$ relation adopted for the Pleiades stars (solid lines), compared with Gray's (2005) empirical relation for dwarfs ($\log g = 4.15 + 0.368(B-V)_0$; dashed line). (d) Adopted ξ vs. $(B-V)_0$ relation corresponding to the empirical $\xi(T_{\rm eff}, \log g)$ formula derived in Paper I (solid line), compared with those of Edvardsson et al. (1993) and Nissen (1981) (dashed lines).

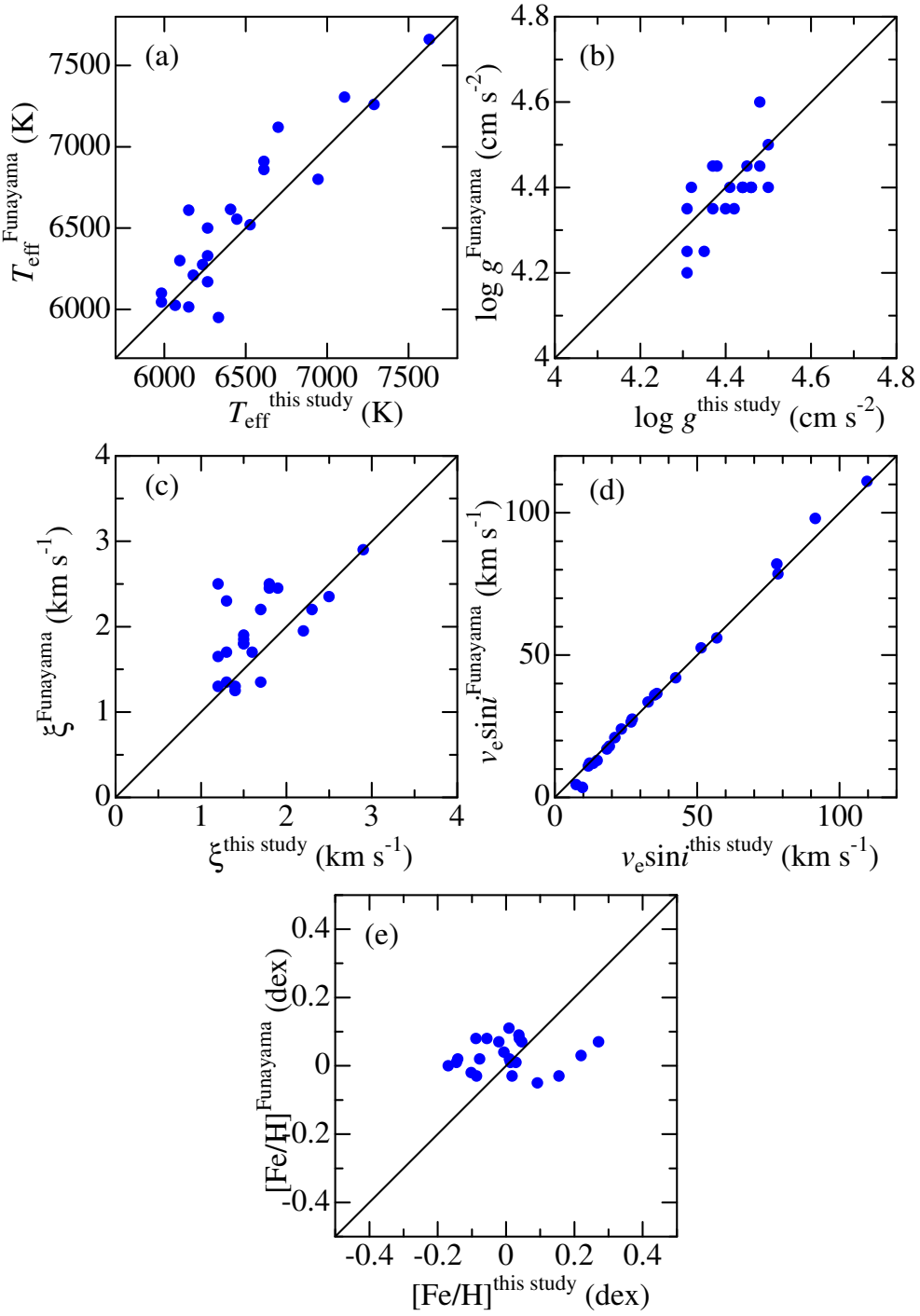

Fig. 2. Comparison of the parameters adopted in this study (as given in table 2) with those derived spectroscopically by Funayama et al. (2009). (a) $T_{\rm eff}$, (b) $\log g$, (c) ξ, (d) $v_{\rm e}\sin i$, and (e) [Fe/H].

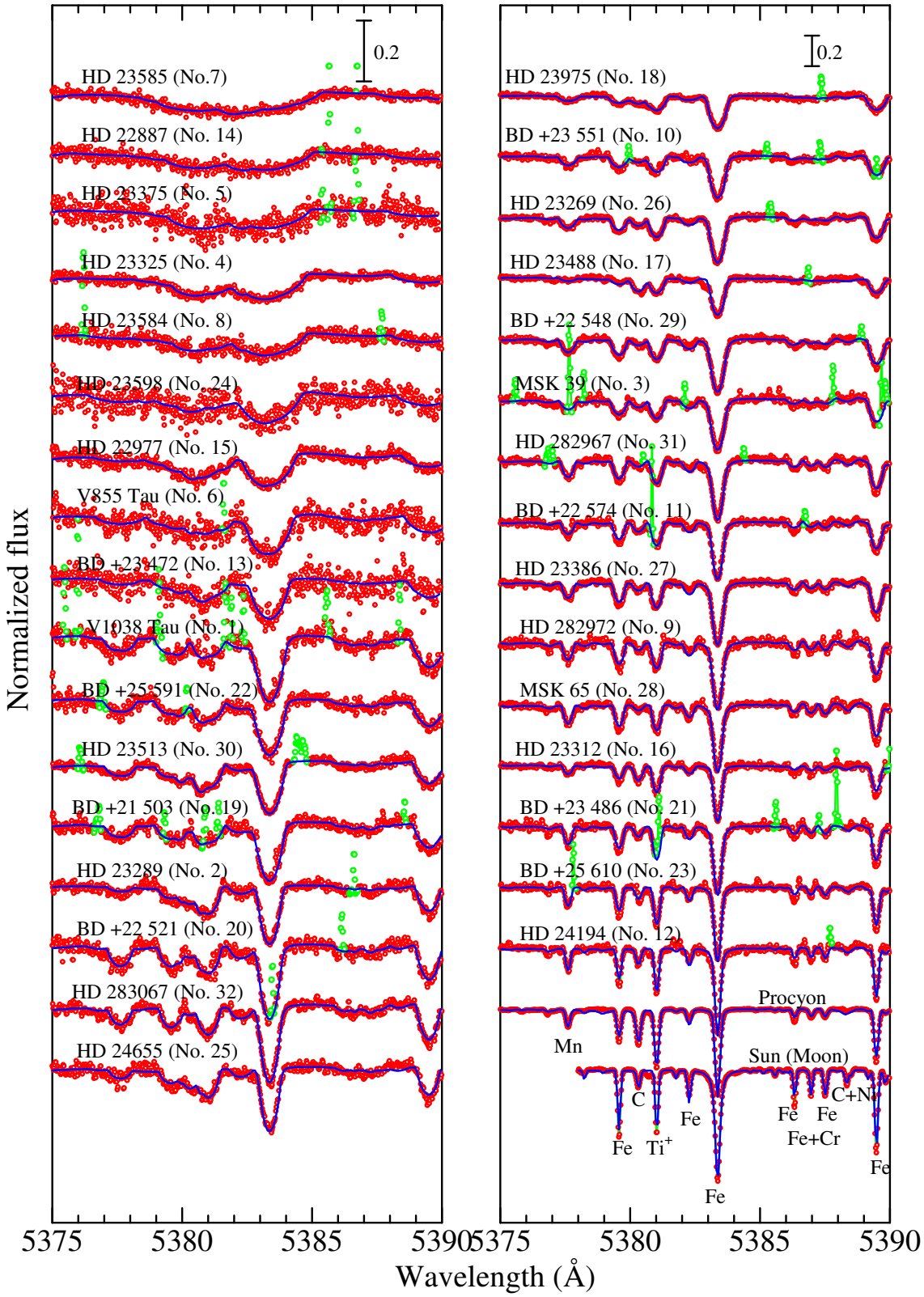

Fig. 3. Synthetic spectrum fitting for the 32 program stars (as well as Procyon and the Sun/Moon) at the 5375–5390 Å region, which was accomplished by adjusting the abundances of C, Ti, Mn, and Fe along with the macrobroadening parameter ($v_{\rm e} \sin i$). The best-fit theoretical spectra are shown by blue solid lines, while the observed data are plotted by red symbols (while those masked/disregarded in the fitting are highlighted in green). In each panel, the spectra are arranged in the descending order of $v_{\rm e} \sin i$ (cf. table 2), and an appropriate offset (0.2 and 0.4 for the left and right panel, respectively) is applied to each spectrum relative to the adjacent one. Note that the vertical scale in the left-had panel is twice as magnified as that of the right-hand panel. The wavelength scale is adjusted to the laboratory frame by correcting the radial-velocity shift.

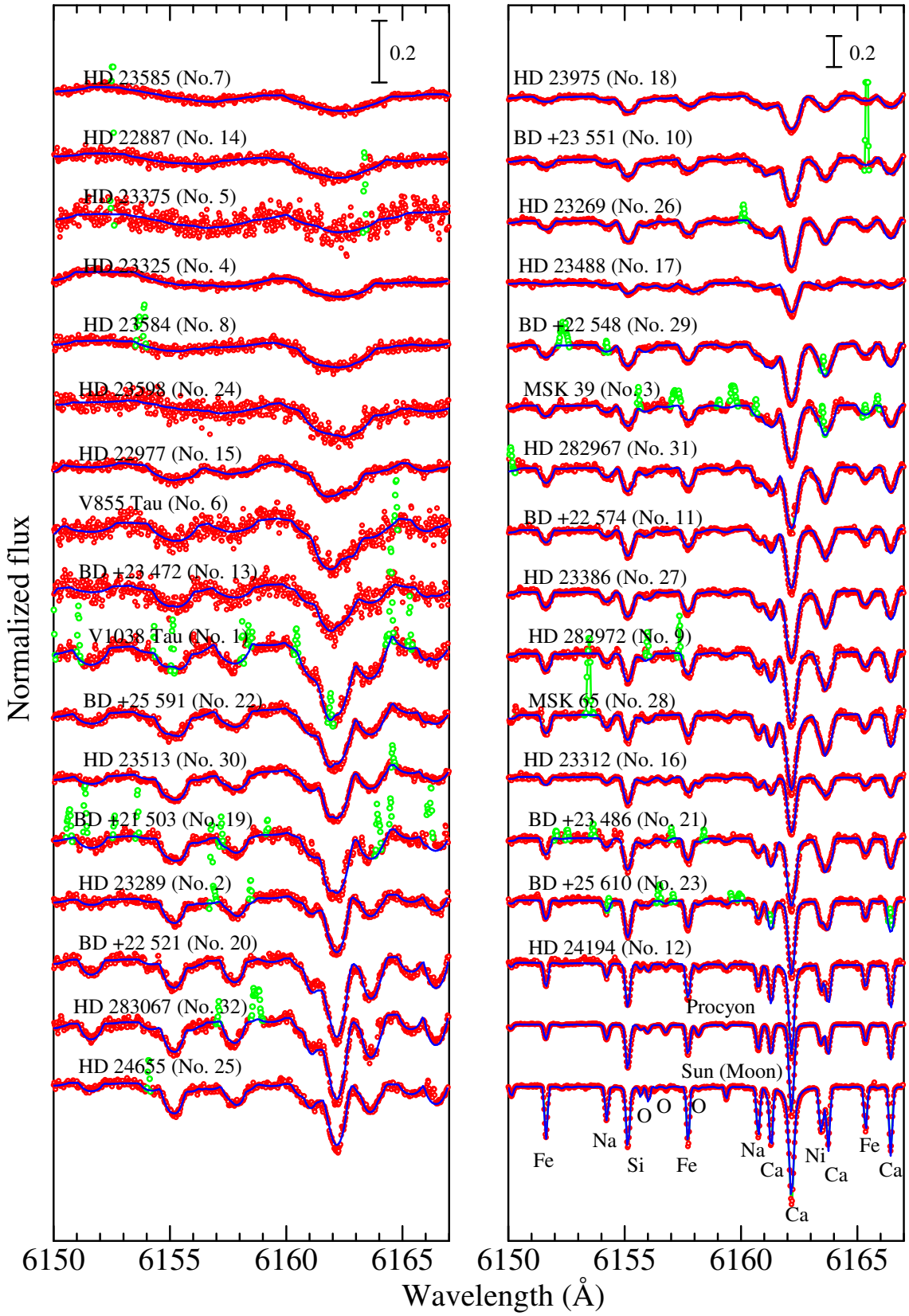

Fig. 4. Synthetic spectrum fitting for the 32 program stars (as well as Procyon and the Sun/Moon) at the 6150–6167 Å region, which was accomplished by adjusting the abundances of O, Na, Si, Ca, Fe, and Ni along with the macrobroadening parameter ($v_e \sin i$). Otherwise, the same as in figure 3.

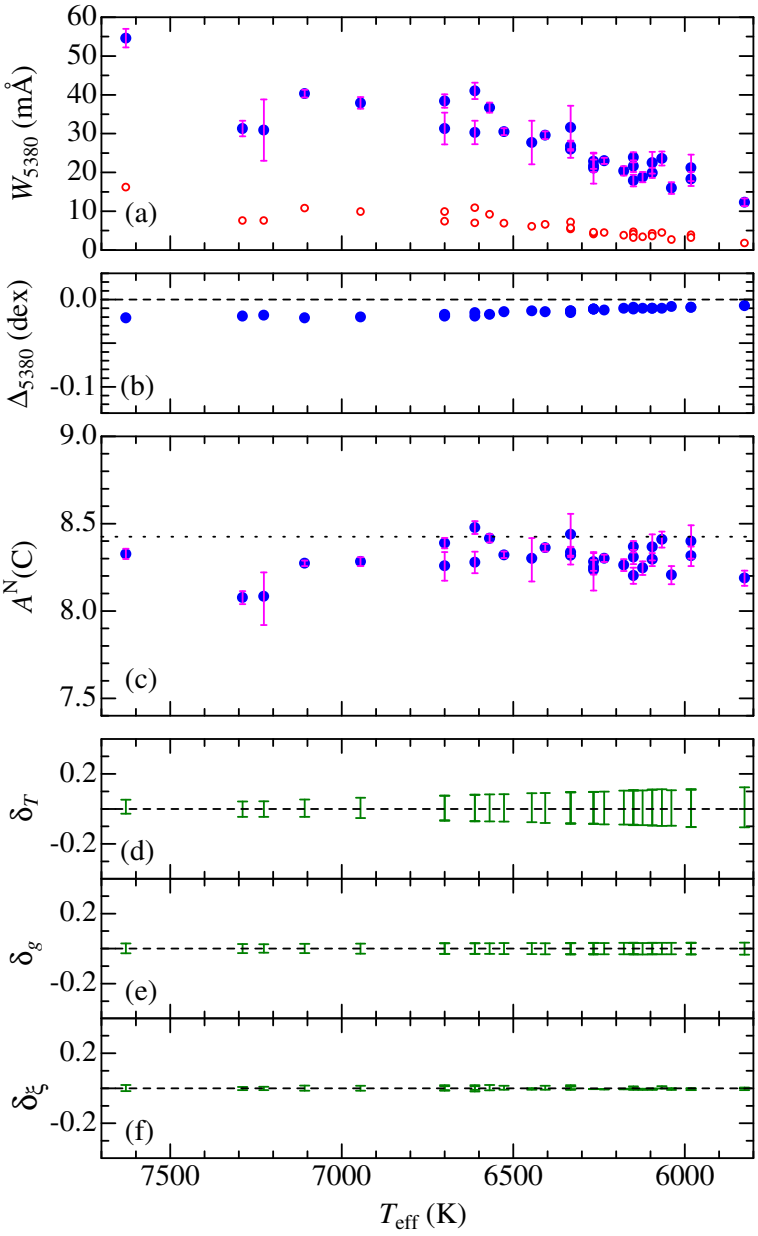

Fig. 5. C I 5380-related quantities plotted against $T_{\rm eff}$. (a) W_{5380} (equivalent width of the C I 5380.325 line [filled symbols] and the C I 5380.227 line [open symbols] inversely computed with the abundance solution derived from fitting), (b) Δ_{5380} (non-LTE correction for the C I 5380.325 line), (c) $A^{\rm N}$(C) (non-LTE abundance derived from $W_{5380.325}$), (d) $\delta_{T\pm}$ (abundance changes in response to $T_{\rm eff}$ variations by $\pm$200 K), (f) $\delta_{g\pm}$ (abundance changes in response to $\log g$ variations by $\pm$0.1 dex), and (g) $\delta_{\xi\pm}$ and (abundance change in response to ξ variations by $\pm$0.5 km s^{-1}). The signs of δ's concerning the variations of $T_{\rm eff}$, $\log g$, and ξ are $\delta_{T+} < 0$, $\delta_{T-} > 0$, $\delta_{g+} > 0$, $\delta_{g-} < 0$, $\delta_{\xi+} < 0$, and $\delta_{\xi-} > 0$. The error bars attached to each of the symbols in panels (a) and (c) denote the S/N-related uncertainties in equivalent widths ($\pm\delta W$) estimated by Cayrel's (1988) relation and the corresponding abundance errors (δ_{W+} and δ_{W-}), respectively. Note that the ordinate scale of panel (b) is as 5 times expanded as that of panels (c)–(f). The dotted line in panel (c) denotes the reference solar C abundance of 8.43 (cf. subsection 4.3).

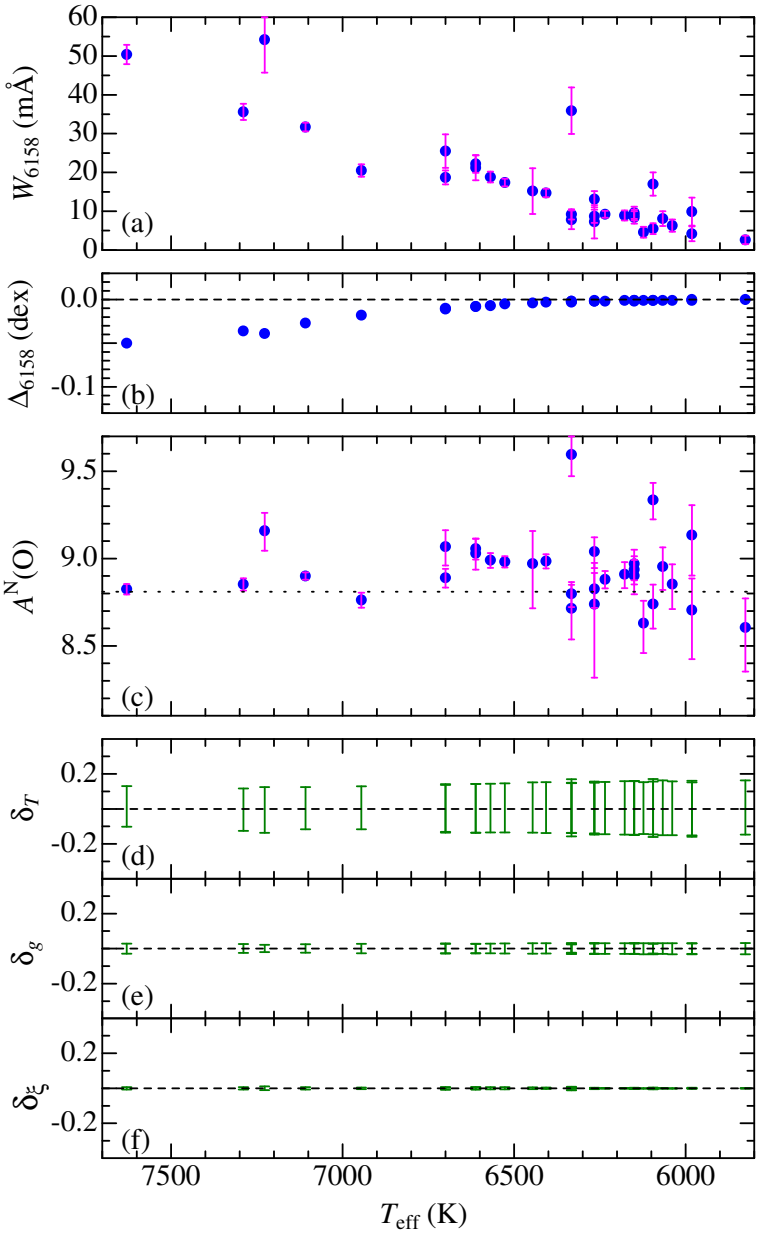

Fig. 6. O I 6158-related quantities plotted against $T_{\rm eff}$. (a) W_{6158} (equivalent width of the O I 6158 line (comprising 3 components) inversely computed with the abundance solution derived from fitting), (b) Δ_{6158} (non-LTE correction for O I 6158), (c) $A^{\rm N}$(O) (non-LTE abundance derived from W_{6158}), (d) $\delta_{T\pm}$ (abundance changes in response to $T_{\rm eff}$ variations by ±200 K), (f) $\delta_{g\pm}$ (abundance changes in response to $\log g$ variations by ±0.1 dex), and (g) $\delta_{\xi\pm}$ (abundance change in response to ξ variations by ±0.5 km s^{-1}). The dotted line in panel (c) denotes the reference solar O abundance of 8.81 (cf. footnote 8). Otherwise, the same as in figure 5.

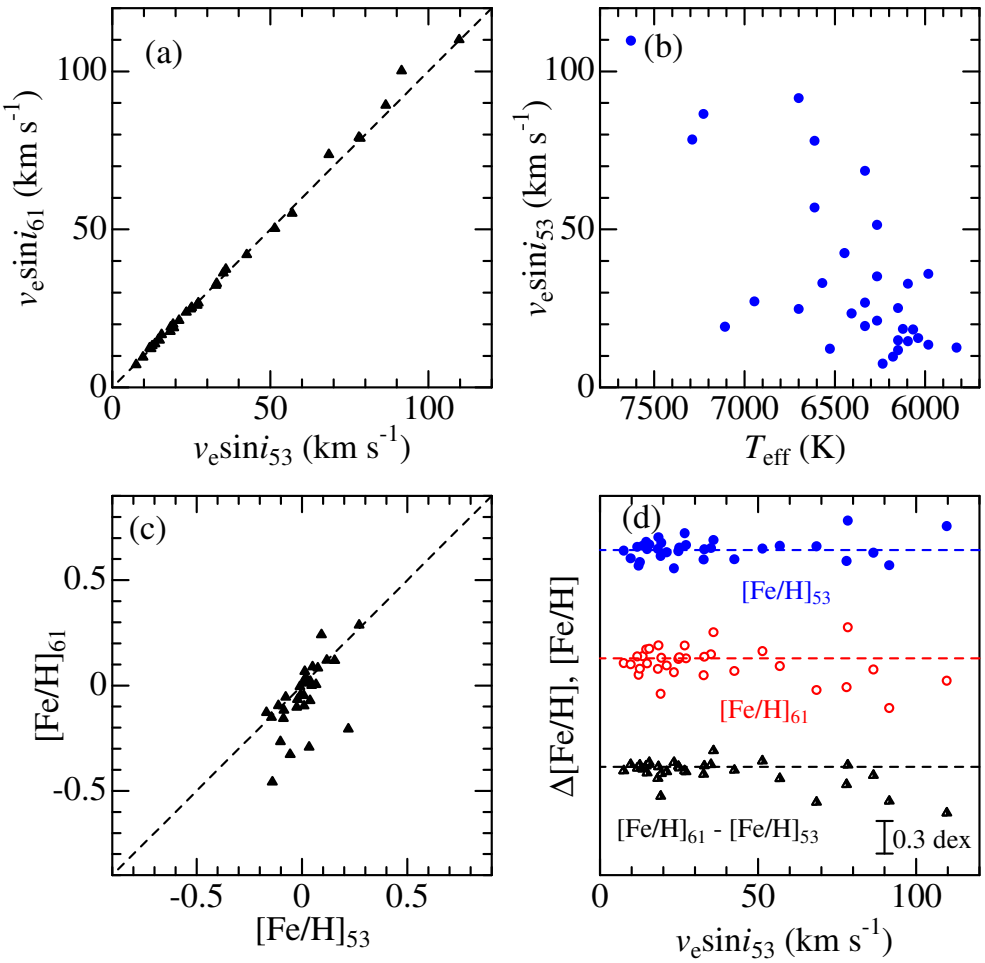

Fig. 7. (a) Comparison of the $v_e \sin i$ values derived from 5375–5390 Å fitting ($v_e \sin i_{53}$; abscissa) with those from 6150–6167 Å fitting ($v_e \sin i_{61}$; ordinate). (b) $v_e \sin i_{53}$ values plotted against $T_{\rm eff}$. (c) Comparison of the [Fe/H] values derived from 5375–5390 Å fitting ([Fe/H]$_{53}$; abscissa) with those from 6150–6167 Å fitting ([Fe/H]$_{61}$; ordinate). (d) [Fe/H]$_{53}$ (upper), [Fe/H]$_{61}$ (middle), and their difference ([Fe/H]$_{61}-$[Fe/H]$_{53}$; lower) plotted against $v_e \sin i_{53}$. The horizontal dashed lines indicate the zero position for each case.

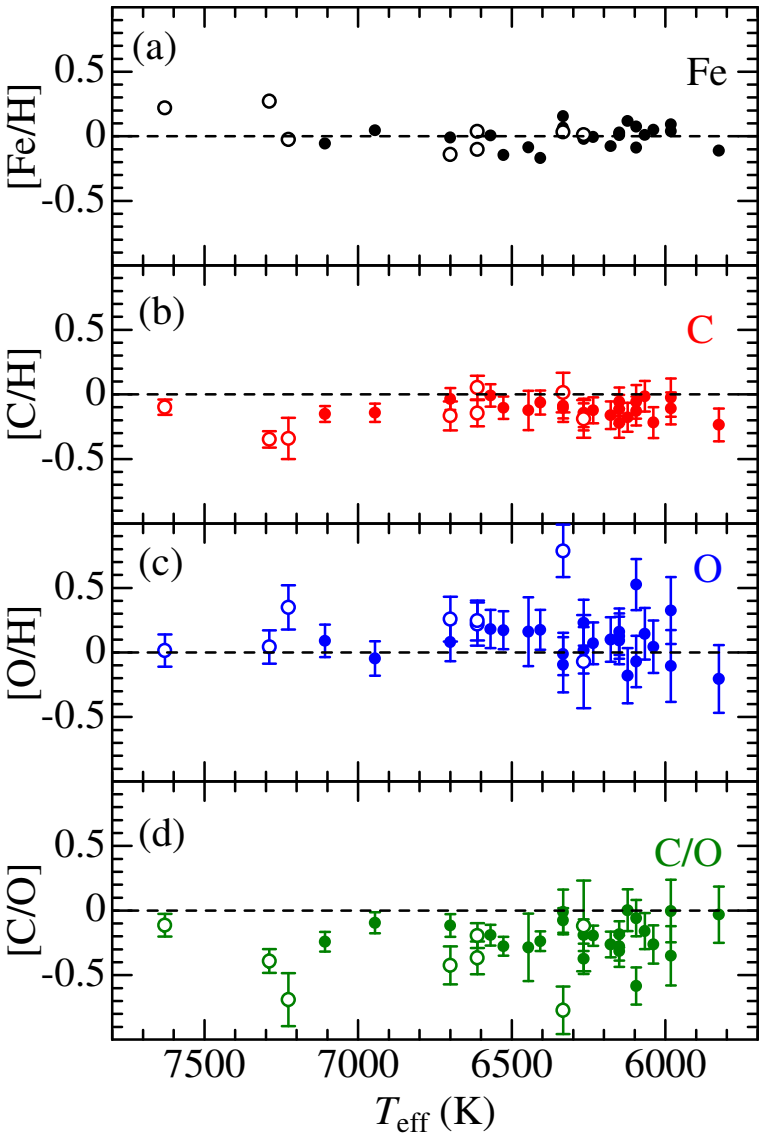

Fig. 8. Logarithmic relative abundances plotted against $T_{\rm eff}$. (a) [Fe/H], (b) [C/H], (c) [O/H], and (d) [C/O] ($\equiv$ [C/H] $-$ [O/H]), based on the data presented in table 2. Filled circles denote stars with $v_{\rm e} \sin i < 50$ km s^{-1}, while open circles correspond to those with $v_{\rm e} \sin i > 50$ km s^{-1}. The error bar ($\pm\delta_{Tg\xi W}$) atached to each symbol in panels (b) and (c) is defined in terms of the quantities introduced in subsection 4.2 (cf. the caption in figure 5) as $\delta_{Tg\xi W} \equiv \sqrt{\delta_T^2 + \delta_g^2 + \delta_\xi^2 + \delta_W^2}$, where $\delta_T \equiv (|\delta_{T+}| + |\delta_{T-}|)/2$, $\delta_g \equiv (|\delta_{g+}| + |\delta_{g-}|)/2$, $\delta_\xi \equiv (|\delta_{\xi+}| + |\delta_{\xi-}|)/2)$, and $\delta_W \equiv (|\delta_{W+}| + |\delta_{W-})|/2$. Meanwhile, the error bar ($\pm\Delta_{Tg\xi W}$) in panel (d) is differently defined (because C/O ratio is concerned and parameter sensitivity tends to be canceled) as: $\Delta_{Tg\xi W} \equiv \sqrt{(\delta_T^{\rm C/O})^2 + (\delta_g^{\rm C/O})^2 + (\delta_\xi^{\rm C/O})^2 + (\delta_W^{\rm C})^2 + (\delta_W^{\rm O})^2}$,, where $\delta_T^{\rm C/O} \equiv (|\delta_{T+}^{\rm C} - \delta_{T+}^{\rm O}| + |\delta_{T-}^{\rm C} - \delta_{T-}^{\rm O}|)/2$, $\delta_g^{\rm C/O} \equiv (|\delta_{g+}^{\rm C} - \delta_{g+}^{\rm O}| + |\delta_{g-}^{\rm C} - \delta_{g-}^{\rm O}|)/2$, and $\delta_\xi^{\rm C/O} \equiv (|\delta_{\xi+}^{\rm C} - \delta_{\xi+}^{\rm O}| + |\delta_{\xi-}^{\rm C} - \delta_{\xi-}^{\rm O}|)/2$.

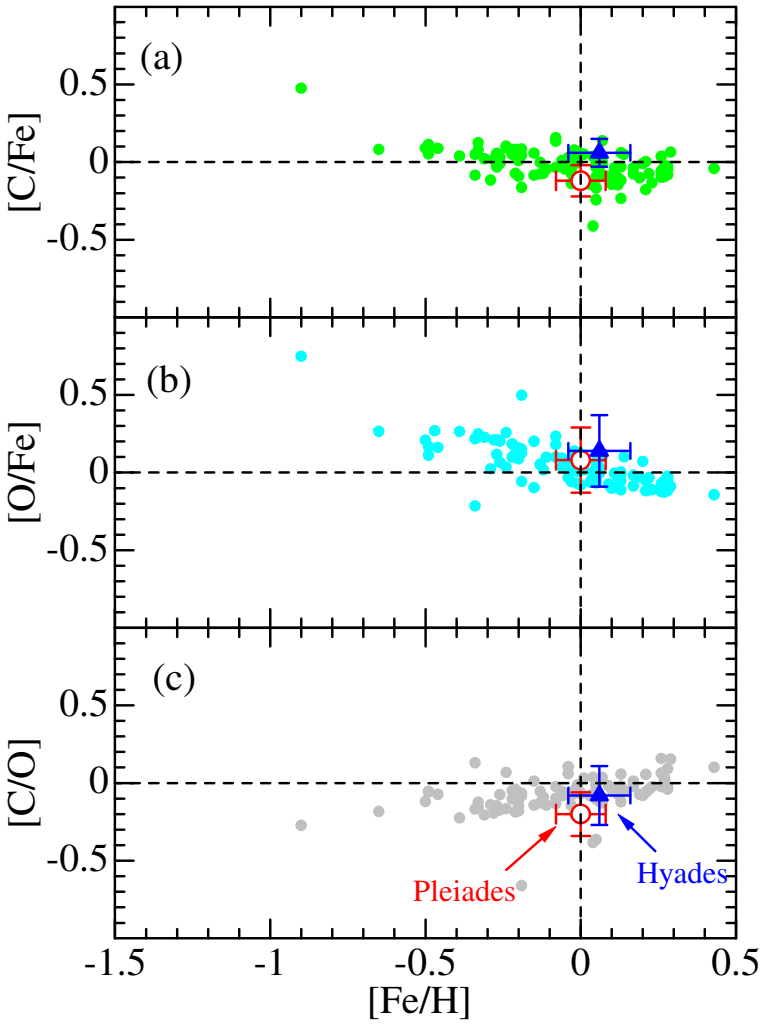

Fig. 9. Distributions of [C/Fe] (upper panel a), [O/Fe] (middle panel b), and [C/O] (lower panel c) plotted against [Fe/H] for Pleiades stars (mean; large open circle; from this study), Hyades stars (mean; large filed triangle; from Paper I) and field F–G stars (small filled circles; from Takeda & Honda 2005). In order to make the three data sets as consistent with each other as possible, the data selections were done according to the following conditions: Pleiades data $\cdots$ stars for $v_{\rm e} \sin i < 50$ km s^{-1}, Hyades data $\cdots$ stars for $T_{\rm eff} > 5800$ K, and field-star data $\cdots$ stars for $T_{\rm eff} > 5800$ K (only data based on C I 5380 and O I 6158 lines were used). The error bars attached to Pleiades and Hyades data denote the standard deviations.

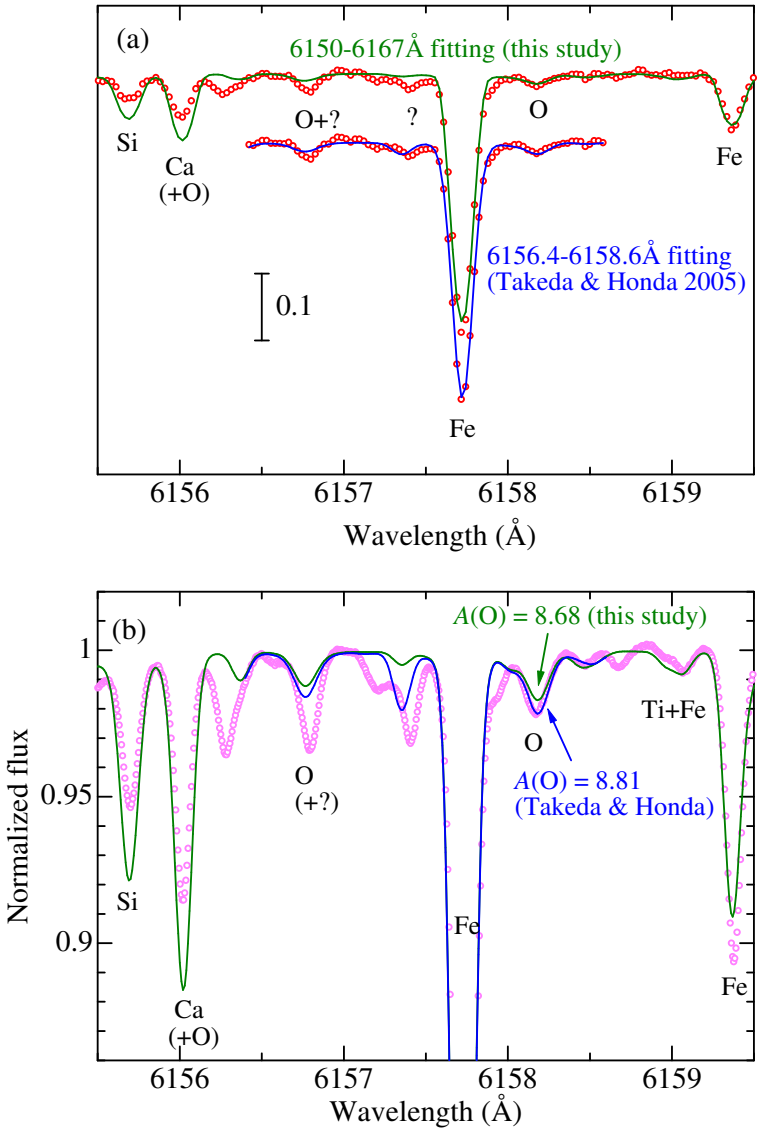

Fig. 10. (a) Comparison of two spectrum fittings in the region of O I 6156–8 lines for solar O abundance determination done in this study (wide 6150–6167 Å region) and in Takeda and Honda (2005) (narrow 6156.4–6158.6 Å region with adjusted strengths of Ti lines to reproduce the 6157.4 Å feature), where open circles and lines represent the Moon spectrum (Takeda et al. 2005a) and the fitted theoretical spectra, respectively. (b) Simulated solar spectra (lines) corresponding to the abundance solutions derived in this study and in Takeda and Honda (2005) (convolved with a Gaussian function with an e-folding width of 2.5 km s^{-1}) in comparison of Kurucz et al.'s (1984) solar flux spectrum (its continuum position is slightly raised by 0.5% in order to match the theoretical spectra).

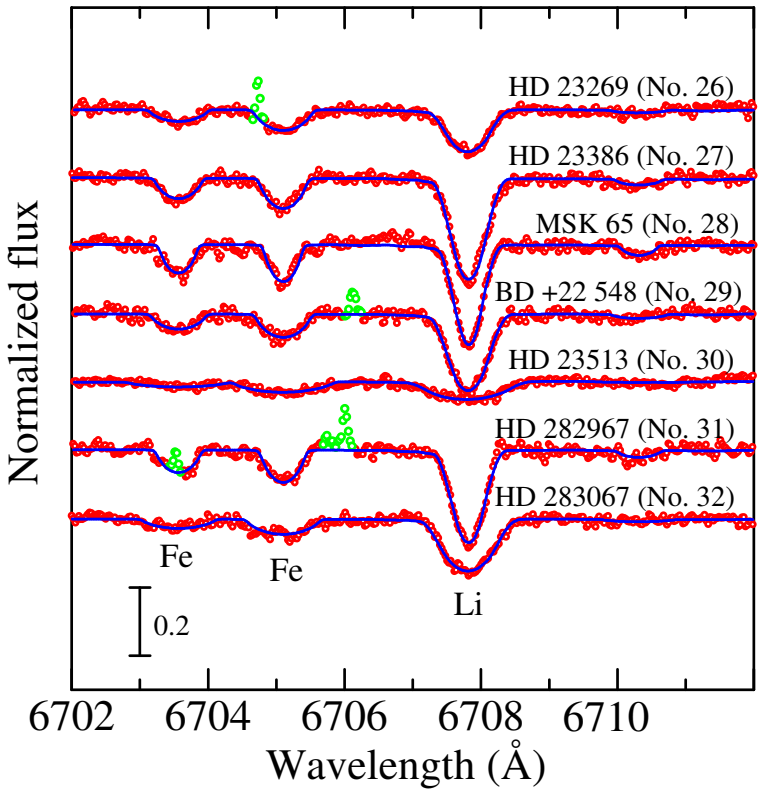

Fig. 11. Synthetic spectrum fitting at the 6702–6712 Å region for 7 stars, for which spectra at the Li I 6708 line are available (i.e., GAOES data in the 2015–2016 season; cf. table 1). The best fit was accomplished by adjusting the abundances of Li and Fe along with the macrobroadening parameter ($v_e \sin i$). The spectra are arranged according to the object number (cf. table 1). An appropriate offset of 0.2 is applied to each spectrum relative to the adjacent one Otherwise, the same as in figure 3.